Introduction

Power amplifiers are one of the most expensive and most power-consuming devices in the communication systems. Digital pre-distortion is an enabling technology for reducing PA cost and improving PA efficiency. With digital pre-distortion the PA linearity is improved and extended so that the PA can be operated at higher power. This means that a lower-power lower-cost linearized PA can be used in place of a higher-power higher-cost PA. Furthermore, the linearized PA operates more efficiently since it is operated closer to saturation. The benefits are compounded because a lower-power PA operating more efficiently consumes substantially less power than an inefficient higher-power PA. The benefits of digital pre-distortion are even more pronounced for multicarrier applications where the peak-to-average power ratio is large. With industry trends towards multicarrier cellular basestations increasing, digital pre-distortion is certain to be a critical technology in the future.

The ISL5239 is a full-featured digital pre-distortion linearizer for power-amplifier linearization. The nonlinear pre-distortion function is defined by a large and highly quantized, programmable look-up table (LUT). The user can choose among three LUT addressing modes to optimize companding. It also includes a novel compensation feature for removing memory effects including those due to thermal variation and self heating, which are a common problem for high-efficiency class AB amplifiers typical of basestation applications.

An on-chip interpolator supports 1x, 2x, 4x, and 8x upsampling. All varieties of upconversion architectures are supported with a programmable correction filter and gain, phase, and offset compensation for direct upconversion, and a digital IF output for heterodyning. Furthermore, the ISL5239 features input and output capture memories along with internal and external triggering capabilities to facilitate closed-loop feedback processing. Figure 1 shows a closed loop digital pre-distortion architecture using the ISL5239.

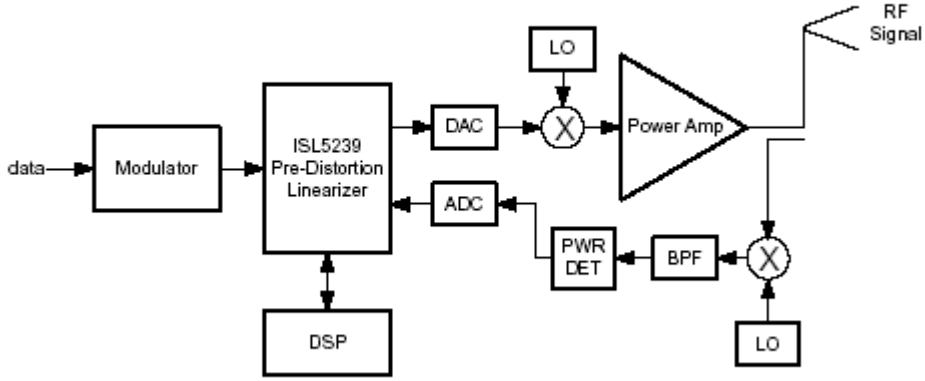

FIGURE 1. CLOSED LOOP DIGITAL PREDISTORTION USING THE ISL5239

The purpose of this application note is to present the features and describe the operation and performance of the ISL5239 PD linearizer.

The application note is organized as follows. In “Linearization Fundamentals” on page 1, we present linearization fundamentals and explain the salient benefits of digital pre-distortion. In “Memoryless Nonlinearity” on page 2, the ISL5239 architecture is presented along with examples demonstrating memoryless linearization performance in several operating modes. The features for memory compensation are presented in“Memory Compensation” on page 18. This section includes examples showing gain-droop correction on pulsed waveforms. The application note concludes with a summary in the “Summary” on page 24.

Linearization Fundamentals

In this section we present the fundamental principles of digital predistortion. We explain how predistortion can be used to linearize a power amplifier (PA) and improve efficiency. We begin by examining the input-output characteristics that govern memoryless PA behavior. A simple polynomial model is presented as an example and then used to explain the concept of intermodulation. Finally, we consider how predistortion can improve PA efficiency.

Memoryless Nonlinearity

As a starting point we consider the linearization of power amplifiers that can be modeled by a memoryless nonlinearity. Figure 2 shows the input-output block diagram of a power amplifier where Vi(t) and Vo(t) are the input and output signals respectively. We consider the complex baseband model in which the output can be expressed as:

$$Vo(t) = g(|Vi(t)|^2)Vi(t) = g_a(|Vi(t)|^2)e^{jg_\Phi(|Vi(t)|^2)}Vi(t) \quad \text{(EQ.1)}$$

where $g_a(|Vi(t)|^2)$ and $g_\phi(|Vi(t)|^2)$ are the amplifier's amplitude and phase transfer characteristics -- commonly referred to as AM-to-AM and AM-to-PM characteristics. This model represents a memoryless nonlinearity because the amplifier characteristics depend only on the instantaneous input power. The input-output relationships can be measured by applying a sinusoidal input and measuring the output amplitude and phase. The amplitude and phase values can be plotted as a function of input power as shown in Figures 3A and 3B. The curves shown in these figures are typical of actual AM-AM and AM-PM measurements, but this data was generated from the polynomial model defined by:

$$g_a(|Vi(t)|^2) = 10 - 10\,|Vi(t)|^2 \quad \text{(EQ.2)}$$

$$g_\phi(|Vi(t)|^2) = -0.3\,|Vi(t)|^2 \quad \text{(EQ.3)}$$

The amplifier's linear characteristic is defined by:

$$\overline{g}_a(|Vi(t)|^2) = 10$$

$$\overline{g}_\phi(|Vi(t)|^2) = 0$$

The linear region is defined as that set of inputs for which $g_a \sim \overline{g}_a$ and $g_\phi \sim \overline{g}_\phi$. From the data in Figure 3, the upper limit of the linear region falls between 5 and 10 dBm. In the linear region of 3A it is evident that the amplifier exhibits a 20 dB gain.

At higher input power levels the amplifier cannot sustain this gain. The 1 dB compression point is defined as the input power at which the amplifier's output power is 1 dB below the linear response. In this case the 1 dB compression point occurs at 20 dBm; that is, with the input power at 20 dBm the output power is 39 dBm, which is 1 dB less than the 40 dBm output power required for linear operation. The saturation point corresponds to the input level that results in the largest output. In this case the saturation point is at 25 dB.

A predistortor preceding the amplifier can be used to linearize the amplifier. For input levels in the linear range of the amplifier, the predistortor applies a gain of 0 dB and has no effect on the signal. In the nonlinear range, the predistortor applies a gain to either amplify or attenuate the input signal. The value of the gain depends on the input level. For example with an input of 20 dBm, the predistortor applies a gain of approximately 2 dB. The amplifier input is now 22 dBm, which results in the desired 40 dBm output. The saturation point defines the upper limit for linearization.

Figure 3B shows the amplifier AM-PM characteristic. At the 1 dB compression point the phase distortion is 2 degrees. At saturation the phase distortion is 7 degrees. Linearization is achieved when the predistortor applies a phase shift that is equal and opposite to that of the amplifier.

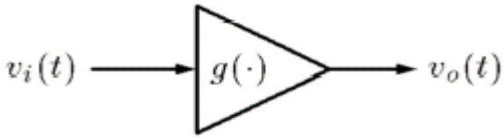

FIGURE 2. POWER AMPLIFIER INPUT-OUTPUT DIAGRAM

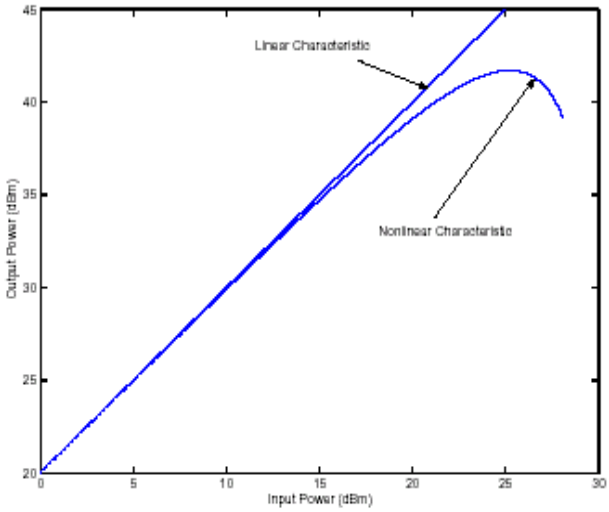

FIGURE 3A. AM-AM CHARACTERISTICS

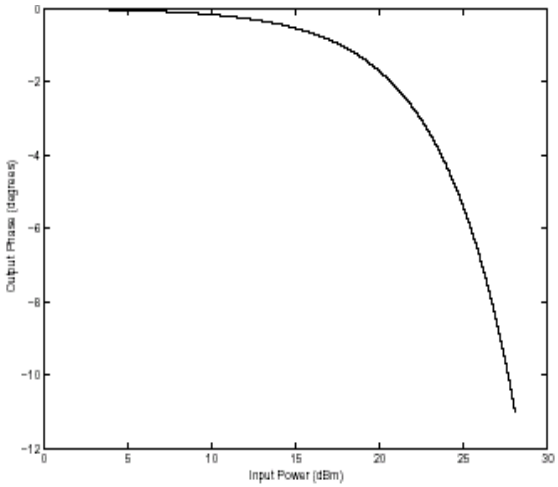

FIGURE 3B. AM-PM CHARACTERISTICS

Intermodulation

Amplifiers are also characterized by their response to inputs constructed from two sinusoidal tones. Consider the two tone input:

$$Vi(t) = Ve^{jw1t} + Ve^{jw2t} \quad \text{(EQ.4)}$$

The input can be expressed using trigonometric identity as:

$$Vi(t) = 2V\cos(w_m t)e^{jwt}$$

where

$$w_m = \frac{w_1 - w_2}{2}$$

and

$$w = \frac{w_1 + w_2}{2}$$

In this form, the two tone input is clearly equivalent to amplitude modulation with a tone and exhibits a peak-to-average ratio (PAR) of 3 dB. Two-tone AM-AM and AM-PM characteristics are sometimes of interest and can be measured. The analysis in [1] suggests that the two-tone 1dB compression point is 2 dB lower than that for a single-tone input. Our interest here is in the amplifier's output spectral response from a two-tone input.

Figure 4A shows the spectrum of the two-tone input signal defined by (4) where w_1 = 5 MHz and w_2 = 9 MHz. In this case the input signal has average power of 17 dBm and a peak power of 20 dBm. The amplifier's amplitude and phase responses given by $g_a(|Vi(t)|^2)$ and $e^{jg\Phi(|Vi(t)|\hat{}2)}$ in (2) and (3) are shown in Figures 4B and 4C respectively. The amplitude response is simply that of double sideband tone modulation. The phase response can be expressed as a Taylor's series:

$$e^{jg_\phi\left(|V_i(t)|^2\right)} = e^{j\alpha 4V^2\cos^2 w_m t}$$

$$= 1 + j\alpha 4vV^2\cos^2 w_m t + \frac{(j\alpha 4V^2\cos^2 w_m t)^2}{2!} + \frac{(j\alpha 4V^2\cos^2 w_m t)^3}{3!} + \ldots$$

where α = -0.3. We can use the identity:

$$\cos^n \omega_m t = \frac{1}{2^n}\binom{n}{\frac{n}{2}} + \sum_{k=1}^{\frac{n}{2}}\binom{n}{\frac{n}{2}-k}\frac{\cos 2kw_m t}{2^{n-1}},\ n = 2, 3, \ldots$$

to write

$$e^{jg_{\phi}\left(|v_i(t)|^2\right)} = C_0 + C_1\cos 2w_m t + C_2\cos 4w_m t + C_3\cos 6w_m t + \ldots$$

where

$$C_0 = 1 + \sum_{m=1}^{\infty} \frac{(j4\alpha v^2)^m}{m!}\binom{2m}{m}\frac{1}{2^{2m}}$$

and

$$C_k = 1 + \sum_{m=k}^{\infty} \frac{(j4\alpha v^2)^m}{m!}\binom{2m}{m-k}\frac{1}{2^{2m-1}},\ k = 1, 2, \ldots$$

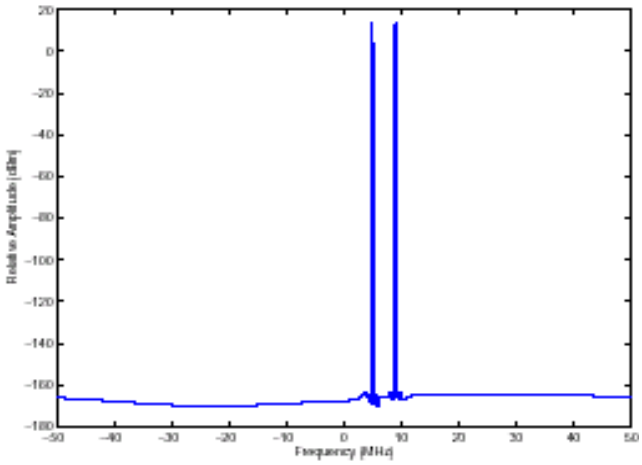

FIGURE 4A. SPECTRUM OF TWO-TONE INPUT (Vi(t))

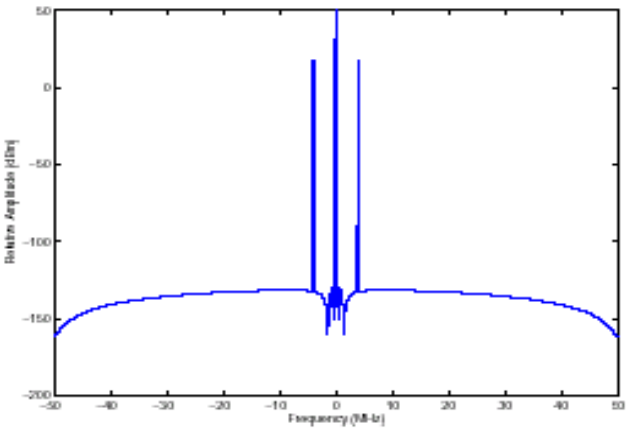

FIGURE 4B. SPECTRUM OF PA AMPLITUDE COMPONENT $g_a(|Vi(t)|^2)$

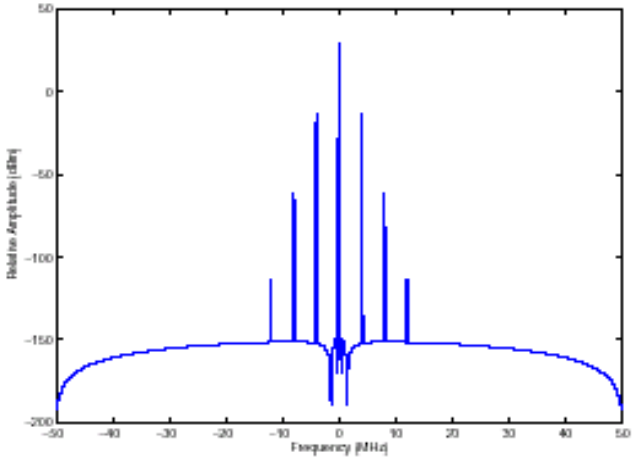

FIGURE 4C. SPECTRUM OF PA PHASE COMPONENT $e^{jg\Phi(|Vi(t)|^2)}$

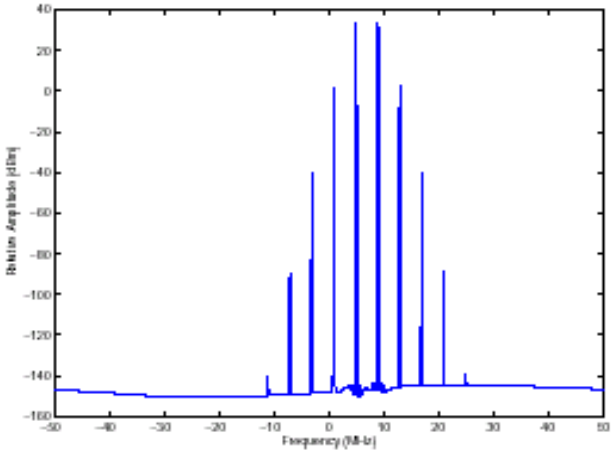

FIGURE 4D. SPECTRUM OF PA OUTPUT Vo(t)

When the amplifier is operated in its linear range, the output spectrum is equal to the input spectrum with a gain of 20 dB. When operated in the nonlinear region, additional spectral components, called intermodulation (IM), are present. The intermodulation components occur at sum and difference frequencies of w_1 and w_2 and their multiples. The IM components of most interest are the third (IM3) and fifth order (IM5) terms which occur at

IM3: $2w_1 - w_2$ and $2w_2 - w_1$

IM5: $3w_1 - 2w_2$ and $3w_2 - 2w_1$

Figure 4D shows IM products that include 7th and 9th order occurring at:

IM7: $4w_1 - 3w_2$ and $4w_2 - 3w_1$

IM9: $5w_1 - 4w_2$ and $5w_2 - 4w_1$

It is evident that the IM products are due to both gain and phase distortion, but phase distortion creates higher-order IM than gain distortion-even though the polynomials for gain and phase distortion have equal order. The intermodulation components of a modulated waveform can be extrapolated from the two-tone analysis. Generally stated, IM3 components interfere with the adjacent channels and IM5 components interfere with both the adjacent and alternate channels as shown in Figure 5. Both IM3 and IM5 cause cochannel interference. Experience has shown that in most cases third- and fifth-order intermodulation components represent the amplifier's dominant distortion components and higher-order terms can be neglected. The pre-distortion bandwidth must be five times the signal bandwidth to cancel the fifth-order intermodulation components.

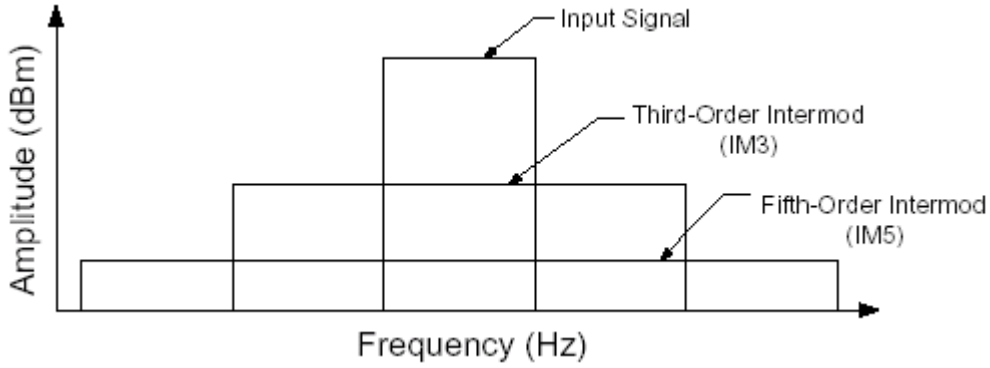

FIGURE 5. INTERMODULATION COMPONENTS

Efficiency

In the above two-tone example where the PAR was 3 dB, the average power of the two-tone signal was 17 dBm and the peak was 20 dBm; that is, the average power was backed off by 3 dB so that the peak power did not exceed the 1 dB compression point of the amplifier. The PAR for multicarrier communication signals can exceed 9 dB PAR and therefore require greater backoff. Unfortunately as backoff increases efficiency decreases.

Figure 6 shows the efficiency of Class A, AB, and B amplifiers as a function of backoff. This data was generated assuming the PA behavior is governed by an ideal strong nonlinearity in transconductance [1]. For an ideal strong nonlinearity, the minimum backoff required for linear operation is equal to the PAR. If we consider a more realistic model that includes a weak nonlinearity, then the backoff needs to be increased by approximately 3 dB. Digital predistortion can be used to linearize the weak nonlinear behavior of the amplifier and reduce backoff by typically 3dB.

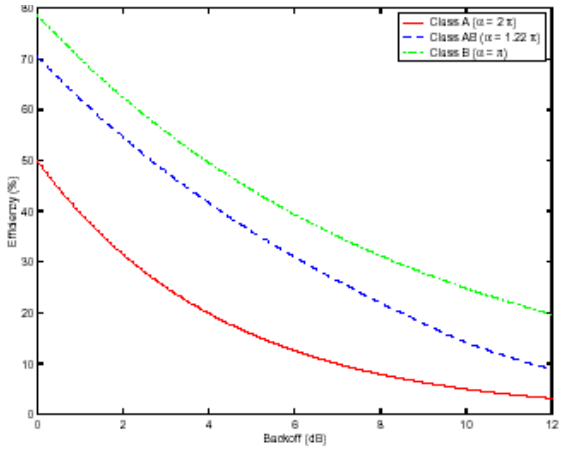

FIGURE 6. AMPLIFIER EFFICIENCY

For example, if the PAR is 9 dB, and we consider an additional 3 dB of backoff for weak nonlinearity, then the total backoff is 12 dB and from Figure 6 this corresponds to class AB efficiency around 9%. If we use predistortion to compensate for the weak nonlinearity and reduce the backoff to 9 dB, then the efficiency climbs to 18%. Table 1 compares PA performance with and without predistortion where the required average transmit power is 10 Watts. Without digital predistortion the backoff is 12 dB, which means a 160 Watt power amplifier is required to satisfy the 10 Watt average transmit power requirement. The efficiency is only 9% which means 111 Watts must be dissipated as heat. With digital predistortion the backoff is only 9dB and a less expensive 80 Watt amplifier meet the 10 W transmit

power requirement. The efficiency rises to 18% with the reduced backoff and the dissipated power is only 55 Watts. With digital predistortion we can use a lower-power lower-cost amplifier and we can operate it more efficiently to substantially reduce the amount of power that must be dissipated at the basestation. This example is based on a set of simplifying assumptions that may not be fully realized in practice, but nonetheless the benefits of digital predistortion are compelling.

TABLE 1. EFFICIENCY AND POWER COMPARISON

DIGITAL PREDISTORTION	NO	YES
AVERAGE TX POWER	10 WATTS	10 WATTS
PAR	9 dB	9 dB
BACKOFF	12 dB	9 dB
PA POWER RATING	160 WATTS	80 WATTS
EFFICIENCY	9%	18%
POWER DISSIPATION	101 WATTS	45 WATTS

Memoryless Linearization

In this section the ISL5239 architecture is presented along with examples demonstrating memoryless linearization performance in several operating modes. We begin by reviewing the features of the ISL5239 including interpolation, addressing mode, IF conversion, correction filter and imbalance compensation. Next we present examples showing linearization performance for a variety of operating modes using a multicarrier CDMA2000 signal.

ISL5239 Architecture

The ISL5239 is a full-featured digital pre-distortion part featuring a high-performance look-up-table-based pre-distortion (PD) processing unit. It includes an interpolator for upsampling and supports all varieties of upconversion architectures with a programmable correction filter for equalization including both sin(x)/x correction and removal of frequency response imbalance between quadrature paths-for example group delay mismatch. Also included are gain, phase, and offset compensation for direct upconversion, and a digital IF output for heterodyning. The ISL5239 features input and output capture memories along with internal and external triggering capabilities that facilitate closed-loop feedback processing.

Figure 7 shows the top-level block diagram of the ISL5239 architecture. The input data is shown at the left of the figure and the output data shown on the right. The part supports a variety of input and output modes including parallel IQ or interleaved IQ in either two's-complement or offset binary formats. The formatting blocks are shown at the input and output ports. The input interpolator shown on the left supports 1x, 2x, 4x, or 8x interpolation. The remaining blocks include the predistortion block, which follows the interpolator, the IF conversion block, the correction filter, and the gain/phase/offset correction block. These blocks require further explanation, and are treated each in turn.

The memoryless predistortion function is shown in Figure 8. The features for memory compensation will be described in “Memory Compensation” on page 18. The LUT features 1024 entries each with a 16 bit unsigned real and 16 bit signed imaginary value. The values in the LUT come from the right half of the complex plane and are uniformly quantized in their real and imaginary parts. Figure 9 shows the region of valid LUT vectors. Overflow can be avoided by restricting vectors to magnitudes below 2^{16} - 1 as shown in the figure.

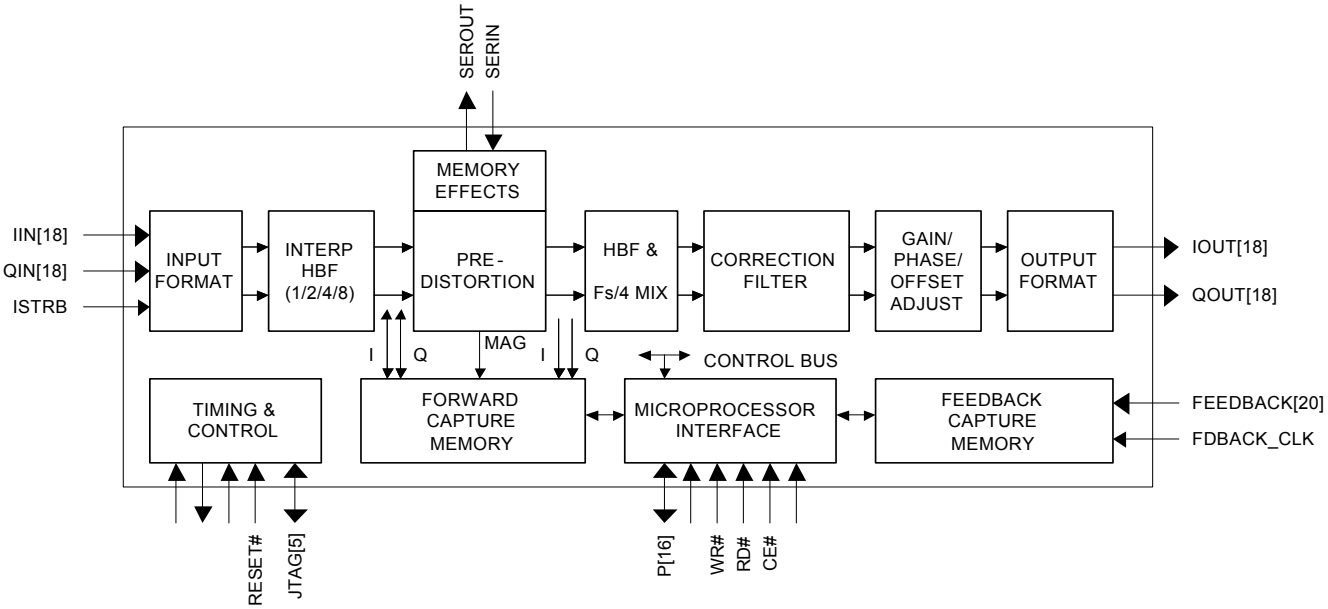

FIGURE 7. TOP LEVEL BLOCK DIAGRAM OF ISL5239

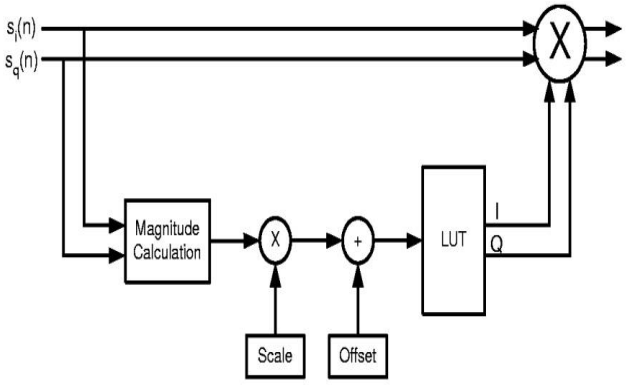

FIGURE 8. MEMORYLESS PREDISTORTION FUNCTION

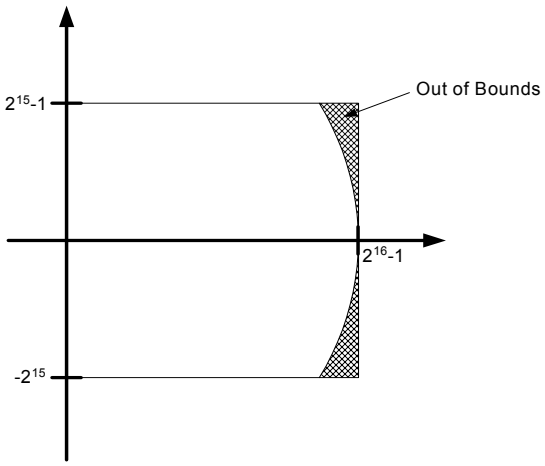

FIGURE 9. LUT SUBSPACE

The ISL5239 provides three addressing modes to support a wide variety of amplifier characteristics. Each mode features different companding properties that govern how the entries in the LUT are distributed across the amplifier's characteristic. The three addressing modes are shown in Figure 10. The multiplexer selects which of the three is used. The upper path into the multiplexer is the linear power mode. The middle path is linear voltage, and the lower path is log power. Figure 11 shows how the LUT entries are distributed for each addressing mode where the scale and offset are normalized. In the linear power mode, all the entries are confined to a range of 30 dB with most entries allocated to the higher power region. All input levels below the 30 dB range are mapped to the first entry in the LUT. This mode is best for amplifiers that exhibits nonlinear behavior only in the upper 30 dB of the characteristic. The linear voltage mode is similar but spans a 60 dB range. The log power mode results in the largest dynamic range. In this mode, the LUT entries are evenly distributed over the input range. For a 120 dB input range, this corresponds to 8.5 entries per dB. The large dynamic range comes with a price: quantization effects can limit performance in this mode if the amplifier characteristic varies significantly over a few dB.

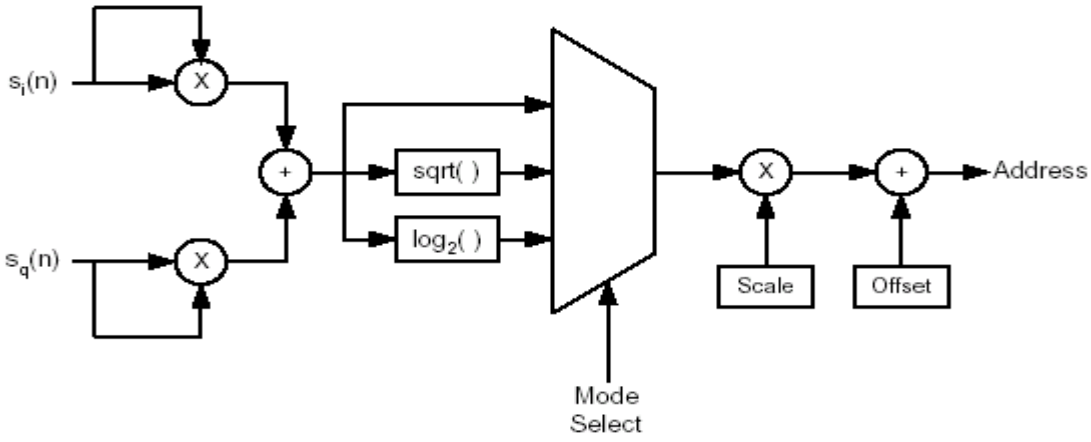

FIGURE 10. ADDRESS CALCULATION

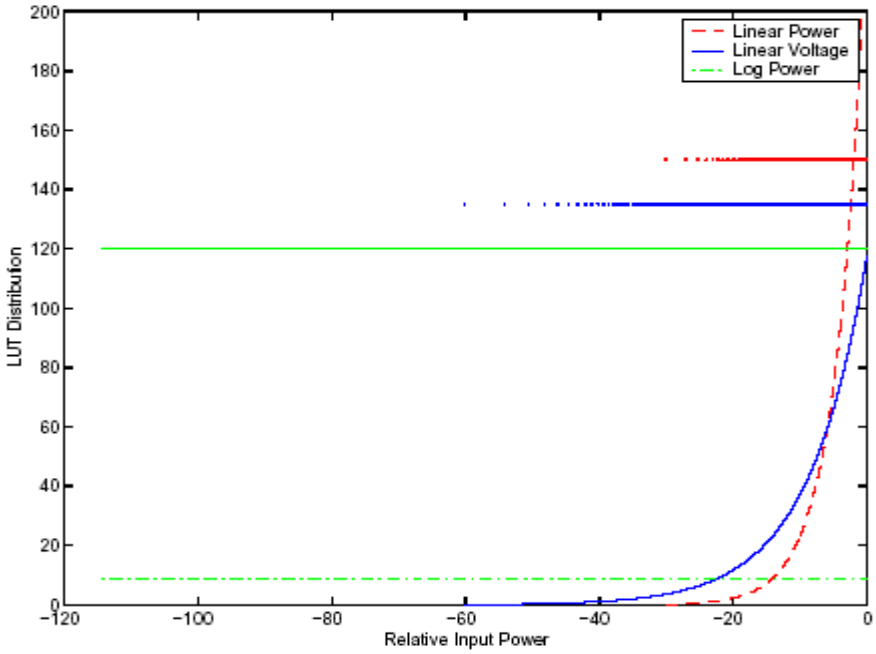

FIGURE 11. DISTRIBUTION OF LUT ENTERIES FOR EACH ADDRESSING MODE

An IF converter follows the predistortor and supports four IF conversion modes: (1) complex zero IF (ZIF); (2) complex Fs/4 IF; (3) real 1x Fs/4 IF; and (4) real 2x Fs/4 IF. The first mode amounts to bypassing the IF converter function. Operation in modes (2), (3), and (4) is shown in Figure 12. In mode (2) the complex input is simply multiplied by $e^{j\pi/4n}$ as shown in Figure 12A. Mode (3) processing is shown in Figure 12B where a half-band filter (HBF) reduces the signal bandwidth by a factor of two before mixing and converting to real. Mode (4), is the same as mode (3) except the sample rate is doubled and the real-valued samples are multiplexed between the I and Q data paths.

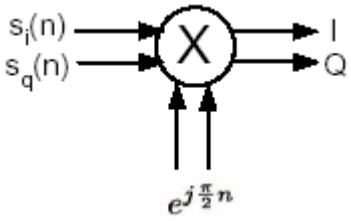

FIGURE 12A. COMPLEX Fs/4 IF UNMUXED

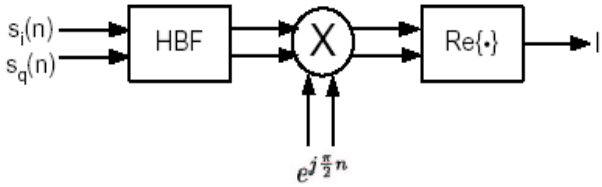

FIGURE 12B. REAL 1X Fs/4 IF UNMUXED

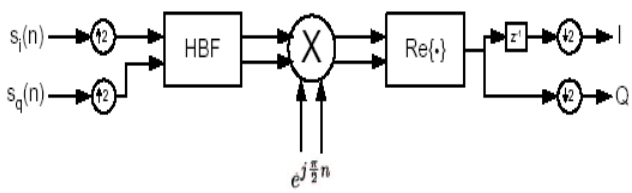

FIGURE 12C. REAL 2X Fs/4 IF MUXED

A programmable correction filter follows the IF converter. The purpose of this filter is to correct for distortion from analog processing including sin(x)/x correction and frequency response imbalance between I and Q channels (either amplitude or group delay). The correction filter operation is dependent on the IF mode as shown in Figure 13.

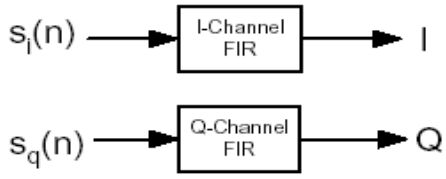

FIGURE 13A. COMPLEX ZIF OR IF UNMUXED

FIGURE 13B. REAL 1X UNMUXED

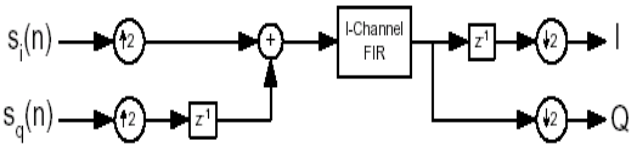

FIGURE 13C. REAL 2X MUXED

The next block includes gain, phase, and DC-offset adjustment for imbalance correction in direct upconversion circuits. An excellent reference that describes techniques for correcting gain, phase, and offset imbalance is [2]. We define the following notation: amplitude gains in the I and Q channels of α and β, phase error of Φ, and DC offsets of a_1 and a_2

The gain imbalance is defined as:

$$\varepsilon = (\alpha / \beta) - 1$$

Typical values are 2-3% for gain imbalance, 2-3 degrees for phase imbalance, and 2-3% full scale for offset imbalance. Figure 14 shows a model of the direct-upconversion circuit along with the ISL5239 compensation function. The ISL5239 output is denoted by:

$$r(t) = \begin{bmatrix} ri(t) \\ rq(t) \end{bmatrix}$$

The direct upconversion output is given by:

$$\begin{bmatrix} Vi(t) \\ Vq(t) \end{bmatrix} = \begin{bmatrix} h_{11} & h_{12} \\ h_{21} & h_{22} \end{bmatrix} \left(\begin{bmatrix} ri(t) \\ rq(t) \end{bmatrix} + \begin{bmatrix} a_1 \\ a_1 \end{bmatrix} \right)$$

where:

$$\begin{bmatrix} h_{11} & h_{12} \\ h_{21} & h_{22} \end{bmatrix} = \begin{bmatrix} a\cos\frac{\Phi}{2} & b\sin\frac{\Phi}{2} \\ a\sin\frac{\Phi}{2} & b\cos\frac{\Phi}{2} \end{bmatrix}$$

A more concise representation is V(t) = H(r(t) + a). The ISL5239 output is given by:

$$\begin{bmatrix} ri(t) \\ rq(t) \end{bmatrix} = \begin{bmatrix} g_{11} & g_{12} \\ g_{21} & g_{22} \end{bmatrix} \begin{bmatrix} si(t) \\ sq(t) \end{bmatrix} + \begin{bmatrix} b_1 \\ b_2 \end{bmatrix}$$

or more concisely as r = Gs(t) + b. The direct upconversion imbalance is corrected when b = -a and $G = H^{-1}$

The ISL5239 includes several other features that are described in detail in the data sheet. This includes input and output capture memories that facilitate adaptive compensation. The capture memories are controlled by either an internal or external trigger. Post and pre-triggering are both supported. The internal triggering mechanism provides a comparator for triggering on the input power level.

Operation and Performance

In this section we present simulation results obtained from a bit-and-cycle accurate model of the ISL5239. In all cases the PA model is that given in Figure 3. We first compare the performance of the three addressing modes for this PA model. Next we investigate the performance of the interpolator. Then we look at gain, phase, and offset compensation along with group delay compensation using the correction filter. Examples are given for each IF mode. Throughout this section data is shown with a spectral resolution bandwidth of 30 kHz.

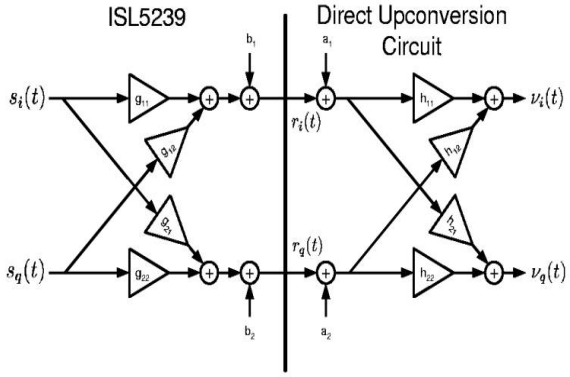

FIGURE 14. IMBALANCE COMPENSATION

Addressing Modes

Figure 15 shows the pre-distortion gain and phase characteristics that linearize the power amplifier from Figure 3. These pre-distortion characteristics were used to generate LUT values for the ISL5239 for all three addressing modes. Figures 16, 17, and 18 compare the linearized gain and phase characteristics that result from each addressing mode. In each case a large improvement in linearization is shown. However, the log power addressing mode does not perform as well as the linear power and linear voltage modes. For the particular pre-distortion characteristic shown in Figure 15, addressing the table in log power distributes fewer LUT entries over the knee region of the pre-distortion characteristic. All three addressing modes show degraded performance at very low input power. For the linear power and linear voltage modes, this is due in part to quantization effects caused by these addressing modes, however, gain and phase performance are particularly sensitive at low input power and degrade as a result of fixed-point limitations unrelated to the LUT addressing mode. This explains the variance of the gain characteristic for log-based addressing at low power shown in Figure 18. Although linear voltage and linear power provide comparable performance, we will limit our examples from this point forward to the linear voltage addressing mode. Very similar results would be expected using the linear power mode, and we make the point that amplifiers exist for which the log power mode is preferred -- in particular amplifiers with gradual nonlinearities that extend over a large dynamic range.

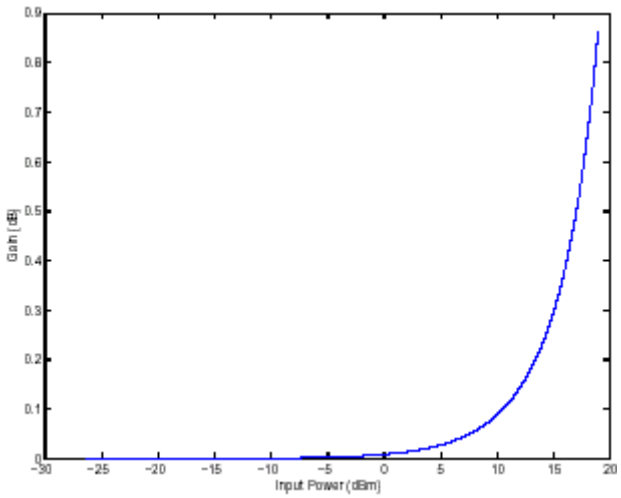

FIGURE 15A. PD GAIN CHARACTERISTIC

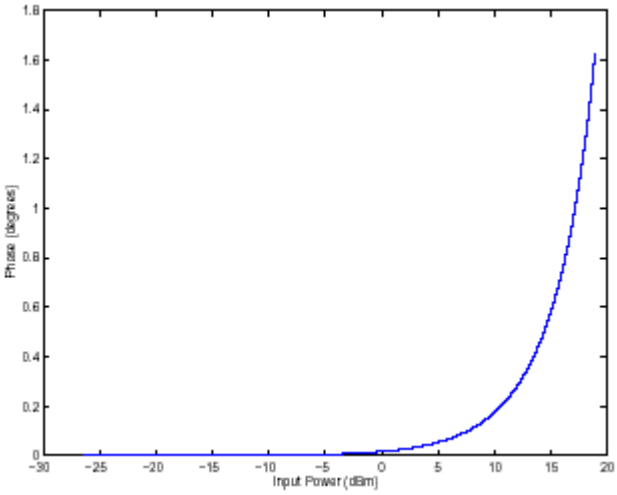

FIGURE 15B. PD PHASE CHARACTERISTIC

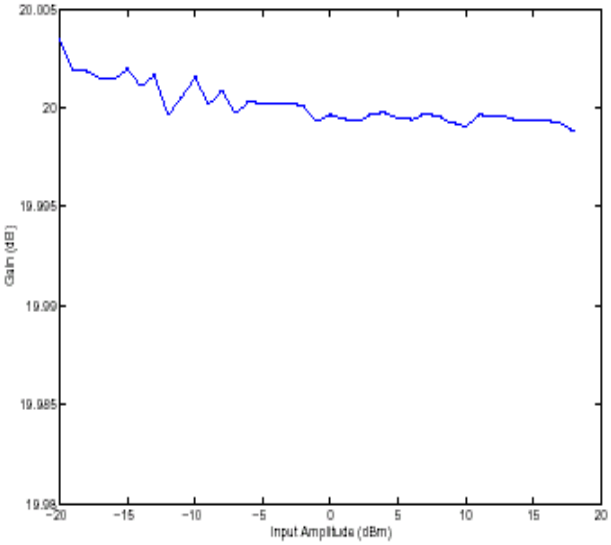

FIGURE 16A. LINEARIZED GAIN (ADDRESSING BY LINEAR POWER)

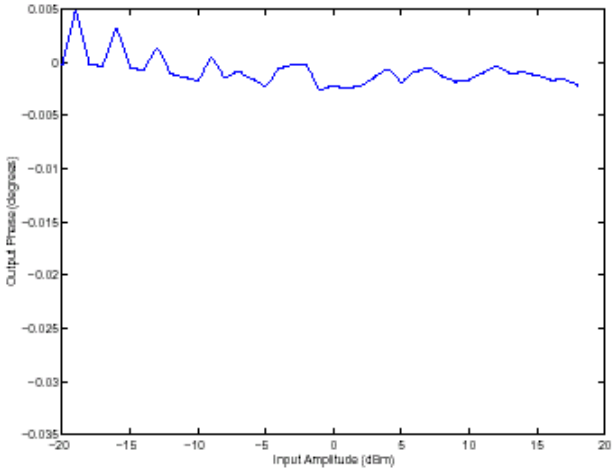

FIGURE 16B. LINEARIZED PHASE (ADDRESSING BY LINEAR POWER)

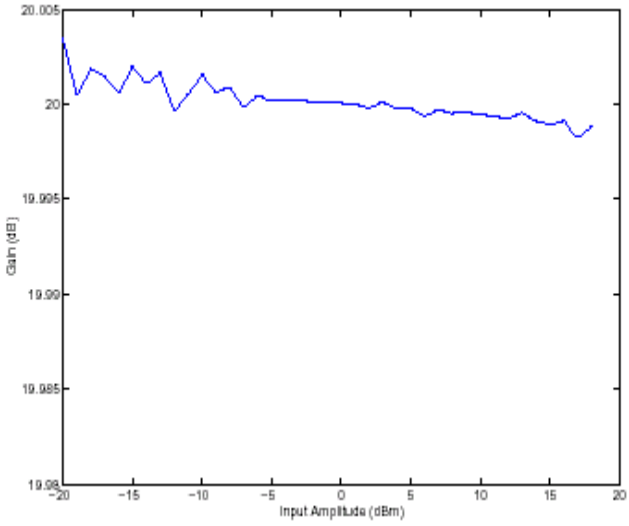

FIGURE 17A. LINEARIZED GAIN (ADDRESSING BY LINEAR VOLTAGE)

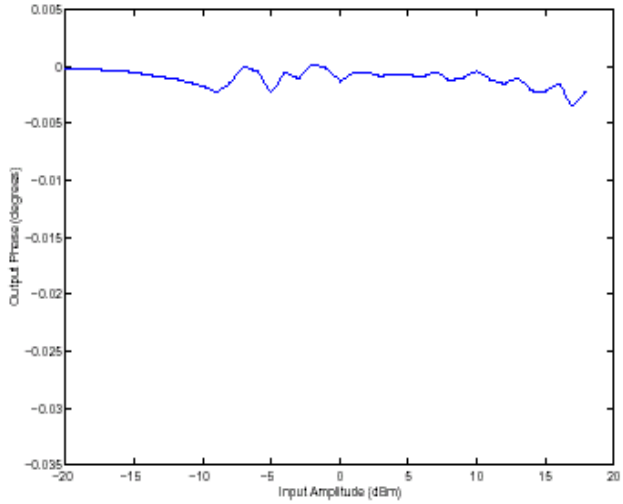

FIGURE 17B. LINEARIZED PHASE (ADDRESSING BY LINEAR VOLTAGE)

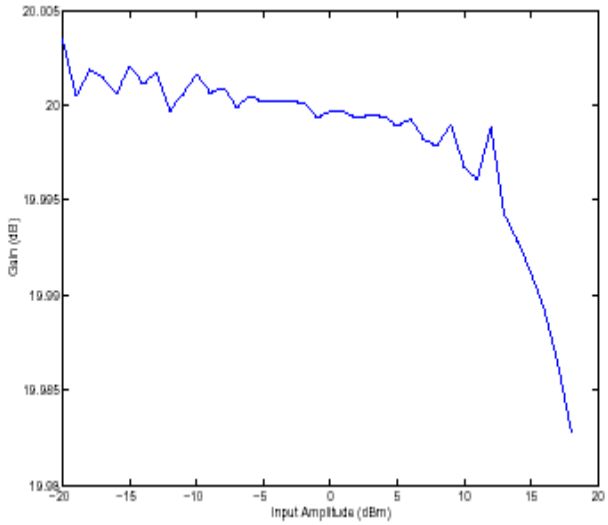

FIGURE 18A. LINEARIZED GAIN (ADDRESSING BY LOG POWER)

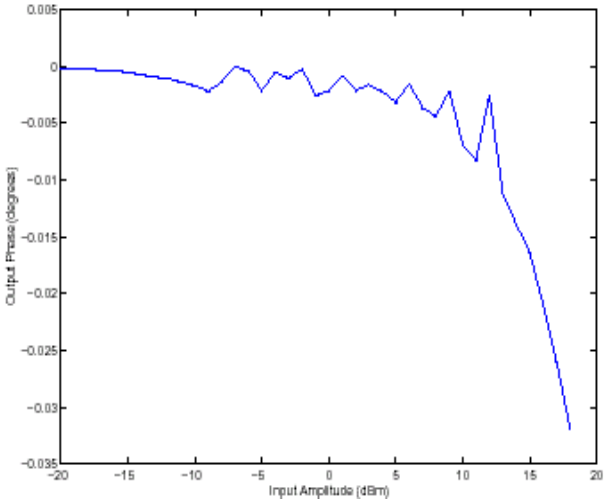

FIGURE 18B. LINEARIZED PHASE (ADDRESSING BY LOG POWER)

Multicarrier CDMA2000

In the remainder of this section, we will use the four-carrier CDMA2000 1X waveform shown in Figure 19 to investigate the performance of the ISL5239. The baseband carriers are centered at -6.25, -3.75, 5.0, and 8.75 MHz. The combined signal has an average power of 10 dBm and a peak power of 20 dBm. This signal is generated with a sampling rate of 29.49 MSPS, or 24 samples per chip. Histograms constructed from 50,000 samples shown in Figure 20 provide estimates of the probability density function (PDF) and the complementary cumulative density function (CCDF).

Figure 21 shows the PA output that results without predistortion. Comparing Figures 21 and 19 it is evident that the output signal has been amplified by 20 dB. However, the output spectrum exhibits large third- and fifth-order intermodulation distortion in the adjacent and alternate bands.

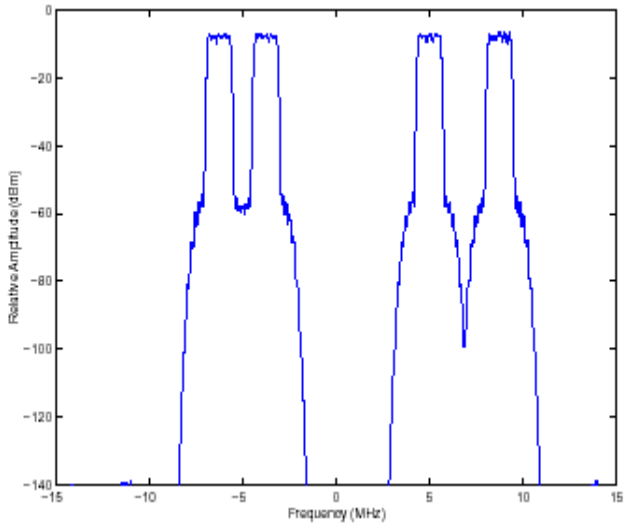

FIGURE 19. FOUR-CARRIER CDMA2000 SPECTRUM

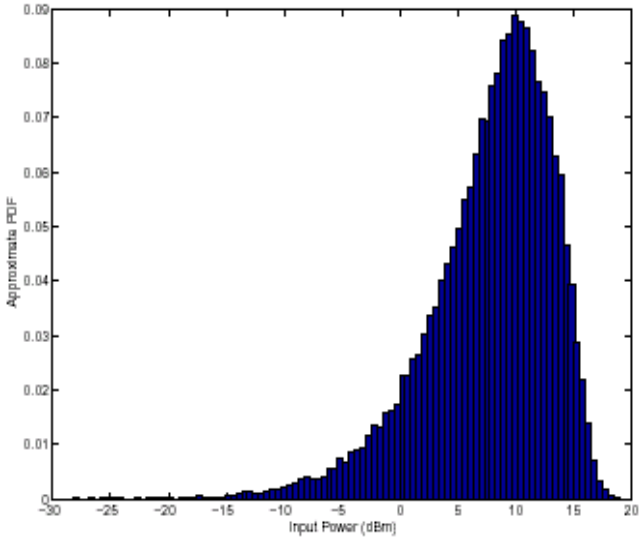

FIGURE 20A. FOUR-CARRIER CDMA2000 WAVEFORM APPROXIMATE PDF

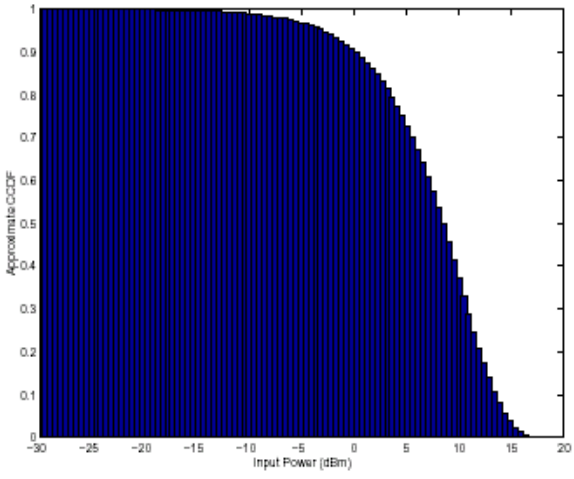

FIGURE 20B. FOUR-CARRIER CDMA2000 WAVEFORM APPROXIMATE CCDF

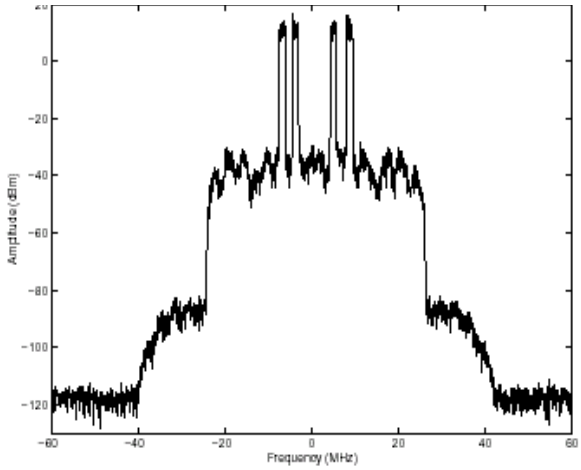

FIGURE 21. OUTPUT WITHOUT PREDISTORTION

Interpolation

Digital predistortion will remove the intermodulation, but performance is dependent on the interpolation factor used in the ISL5239. Figure 22 shows the interpolator output for 1x, 2x, 4x, and 8x factors. Comparing Figures 22A, 22B, 22C, and 22D it is evident that as the sampling rate increases the noise floor decreases. It is well known that each time the sampling rate is doubled, the effective quantization level increases by one-half of a bit-or 3 dB. Note that the sampling rate for 8x interpolation (Fs = 240 MHz in this case) is beyond the capability of the ISL5239 (Fs ≤125 MHz), but is included here for comparison purposes.

Figure 23 shows the PA output when predistortion is used at each interpolation rate. Figures 23A and 23B show that the 1x and 2x interpolation rates are not sufficient for correcting IM distortion in this case. Figures 23C and 23D show acceptable predistortion performance at the 4x and 8x rates. The 4x rate requires a sample rate of 120 MHz and is realizable by the ISL5239, but the 8x rate requires a 240 MHz sample rate and is beyond the capability of the ISL5239 in this case. From this point forward, we will use the 4x interpolation rate.

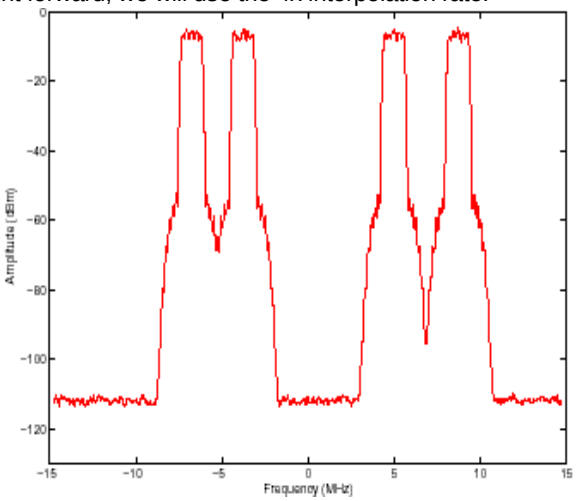

FIGURE 22A. 1X RATE (Fs = 30 MHz)

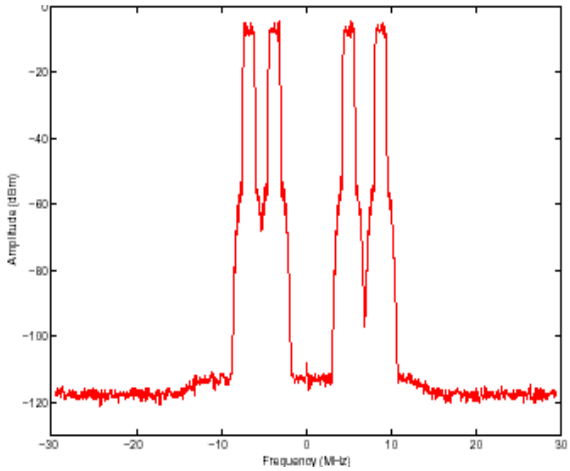

FIGURE 22B. 2X RATE (Fs = 60 MHz)

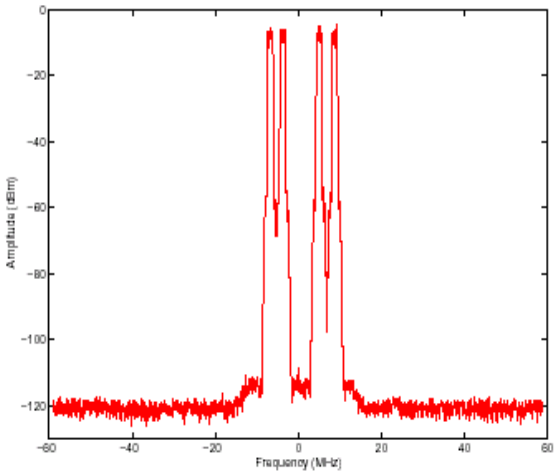

FIGURE 22C. 4X RATE (Fs = 120 MHz)

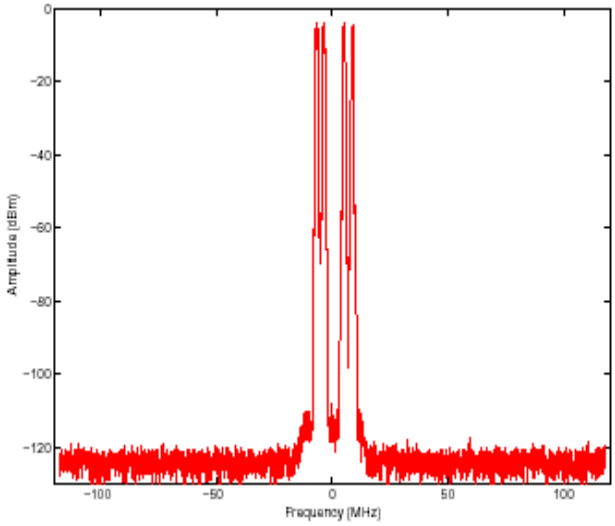

FIGURE 22D. 8X RATE (Fs = 240 MHz)

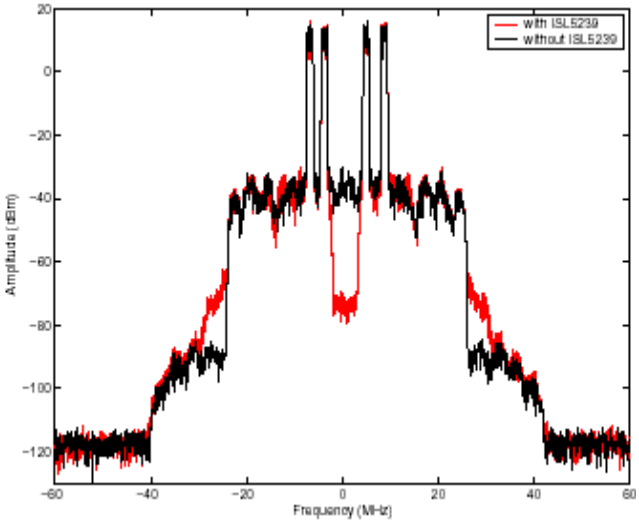

FIGURE 23A. PD PERFORMANCE AT 1X RATE

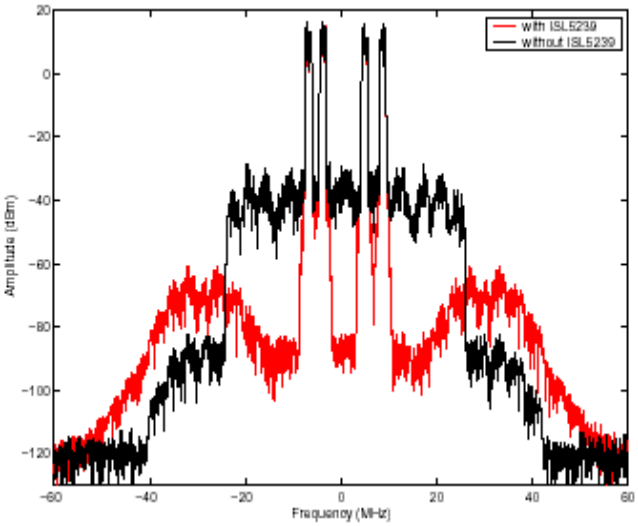

FIGURE 23B. PD PERFORMANCE AT 2X RATE

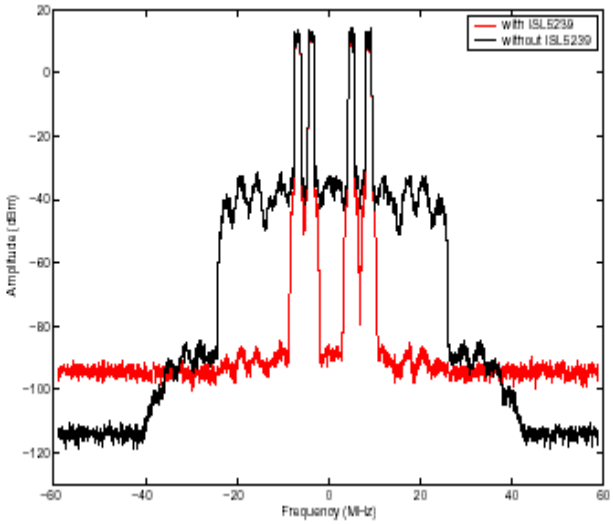

FIGURE 23C. PD PERFORMANCE AT 4X RATE

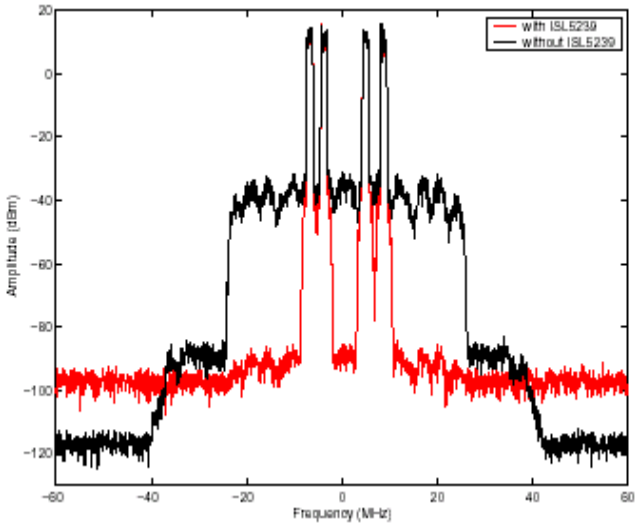

FIGURE 23D. PD PERFORMANCE AT 8X RATE

Direct Upconversion

Direct upconversion circuits exhibit gain, phase, and offset imbalance as discussed in earlier section. We consider each impairment individually and then jointly starting with gain imbalance. Figure 24A shows the predistortion performance when the gain offset is 3%. This figure shows both a severe degradation in IM correction along with poor image rejection by the direct upconverter due to gain imbalance. Figure 24B shows the predistortion performance with gain imbalance correction.

Figure 25A shows the performance with a 3 degree phase imbalance. The distortion from phase imbalance is very similar to that from gain imbalance. Figure 25B shows the performance with phase imbalance correction.

Figure 26A shows the performance with a 3% offset imbalance. The distortion from offset imbalance appears as a DC spike in the spectrum along with IM distortion due to a shift in the PA input magnitude. Figure 26B shows the performance with offset imbalance correction.

Figure 27A shows the performance with all three types of distortion. The IM distortion is very severe when all three imbalance terms are included. However, Figure 27B shows that even this severe distortion can be corrected.

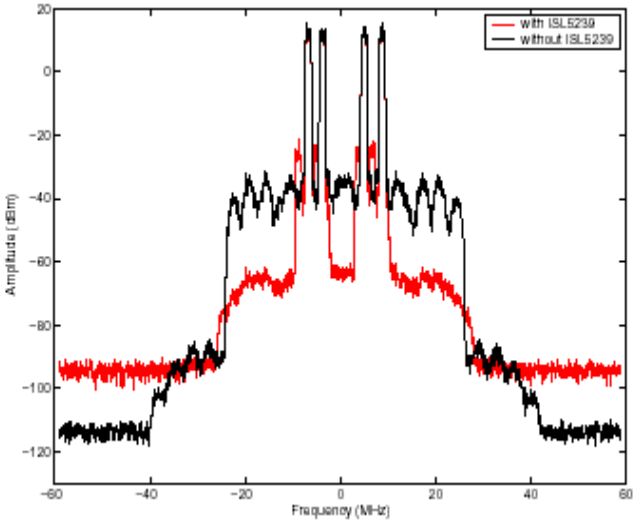

FIGURE 24A. 3% GAIN IMBALANCE WITHOUT CORRECTION

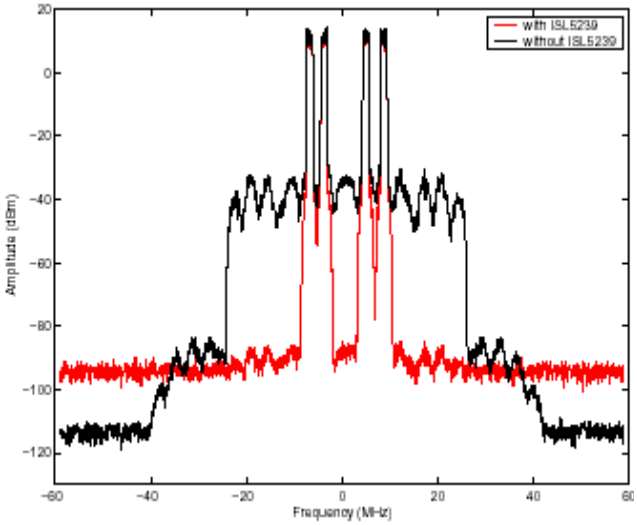

FIGURE 24B. 3% GAIN IMBALANCE WITH CORRECTION

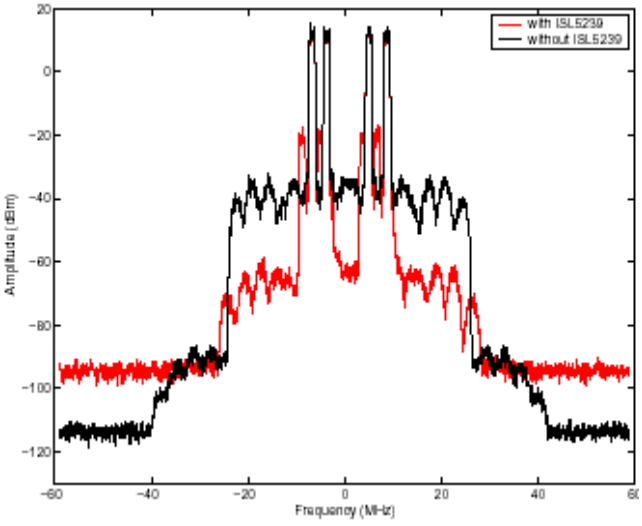

FIGURE 25A. 3 DEGREE PHASE IMBALANCE WITHOUT CORRECTION

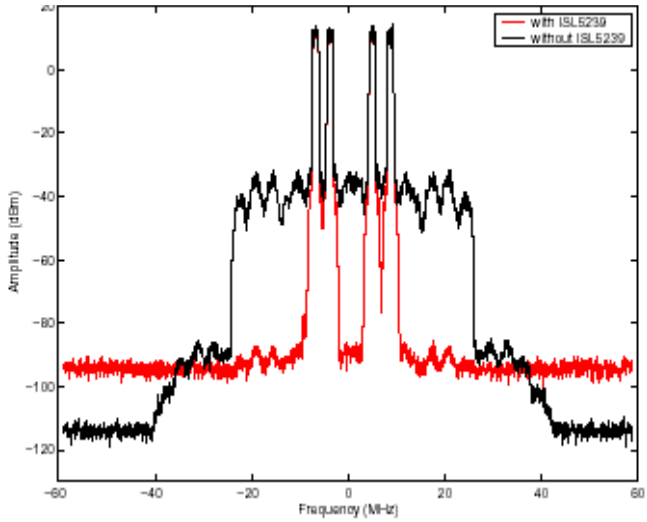

FIGURE 25B. 3 DEGREE PHASE IMBALANCE WITH CORRECTION

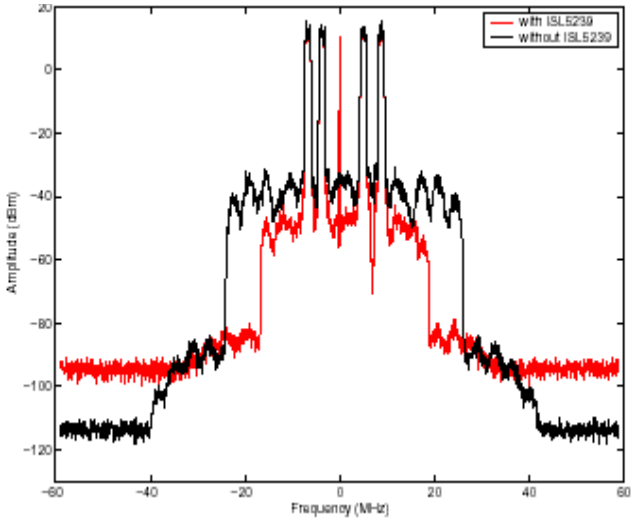

FIGURE 26A. 3% OFFSET IMBALANCE WITHOUT CORRECTION

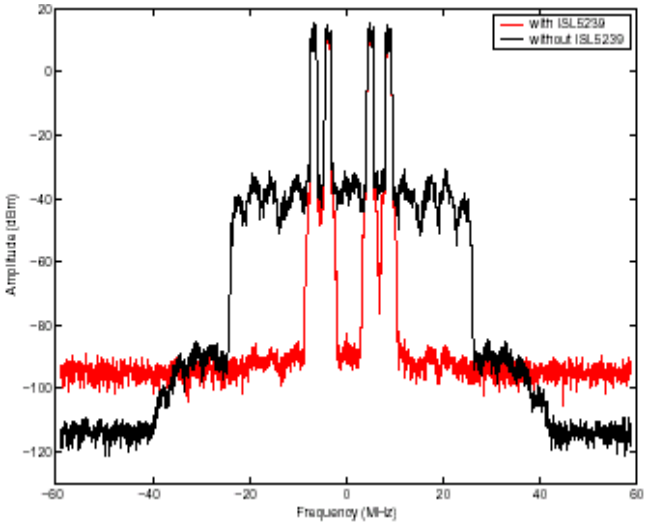

FIGURE 26B. 3% OFFSET IMBALANCE WITH CORRECTION

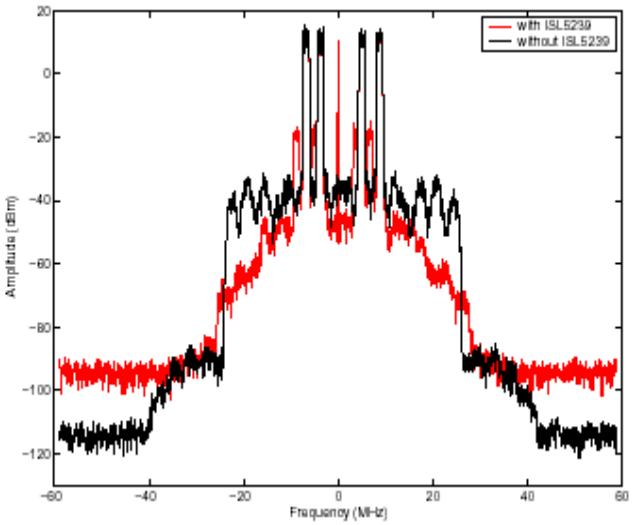

FIGURE 27A. GAIN, PHASE AND OFFSET IMBALANCE WITHOUT CORRECTION

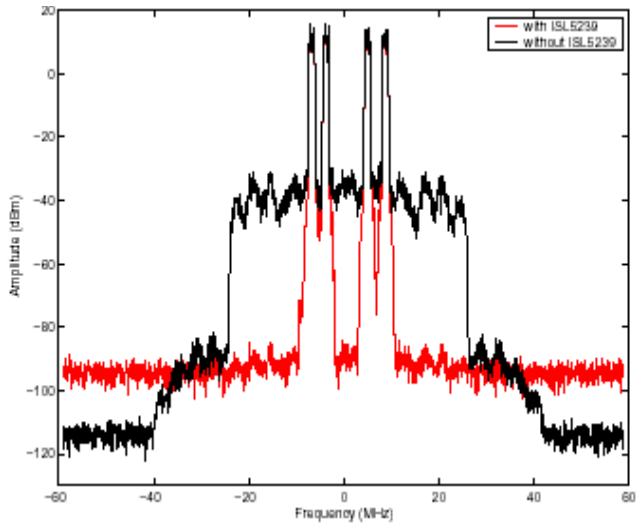

FIGURE 27B. GAIN, PHASE AND OFFSET IMBALANCE WITH CORRECTION

Correction Filter

Another problem with direct upconversion is frequency response imbalance between the I-and Q-channels. This imbalance can appear in gain, phase, or group delay. In the beginning of this section the ISL5239 programmable correction filter was described. This filter can be used to remove frequency response imbalance. Figure 28 shows frequency response mismatch between I- and Q-channels caused by filter component mismatch. This example represents worst case imbalance for components within 2% tolerance. The filter transition band at 60 MHz is evident from the figure.

Figure 29 shows the correction filter that results in minimum mean-square error across 80% of the digital bandwidth. Figure 30 shows the total response of the correction filter in cascade with the analog filter. The correction filter performance is excellent at low frequencies but degrades in the neighborhood of the transition band at 60 MHz and beyond.

Figure 31A shows how the frequency response imbalance shown in Figure 28 can effect PD performance. Figure 31B shows the performance with the correction filter.

Figure 32A shows the response suffering from combined gain, phase, offset, and frequency response imbalance. Figure 32B shows the response when we correct for these imbalances.

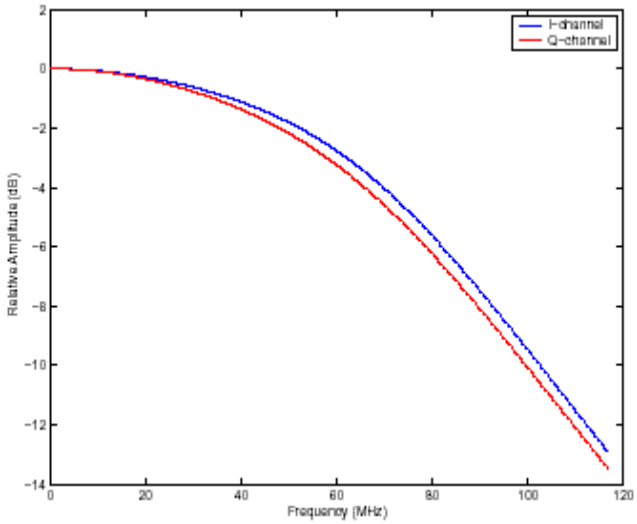

FIGURE 28A. GAIN RESPONSE IMBALANCE

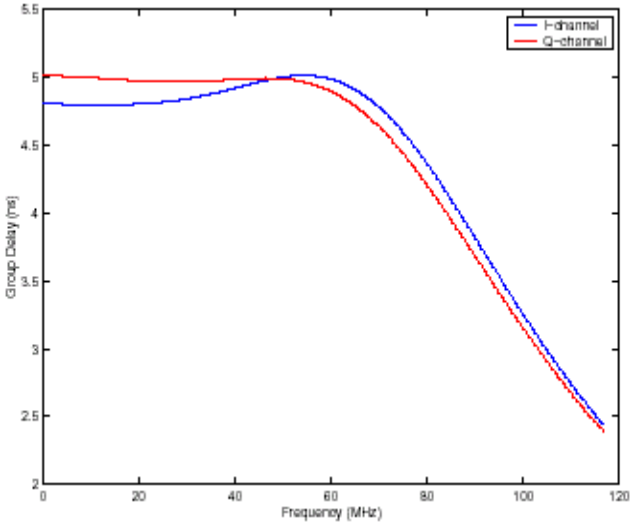

FIGURE 28B. GROUP DELAY IMBALANCE

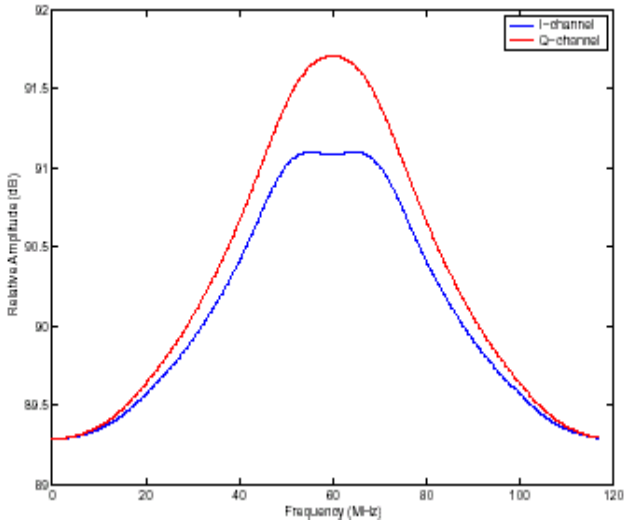

FIGURE 29A. I-CHANNEL CORRECTION FILTER RESPONSE

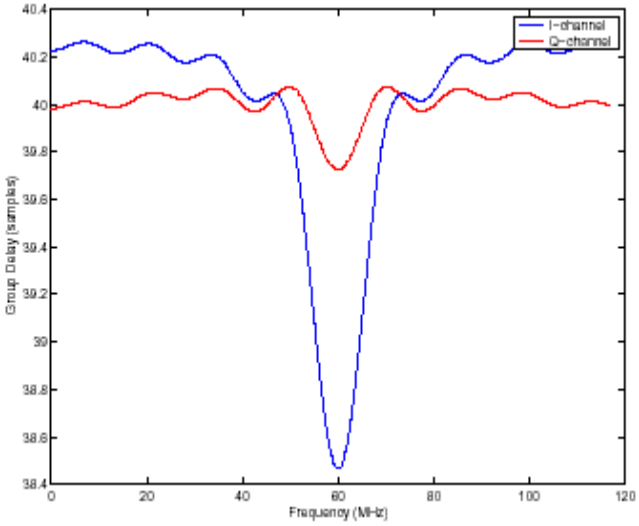

FIGURE 29B. I-CHANNEL CORRECTION FILTER FREQUENCY RESPONSE

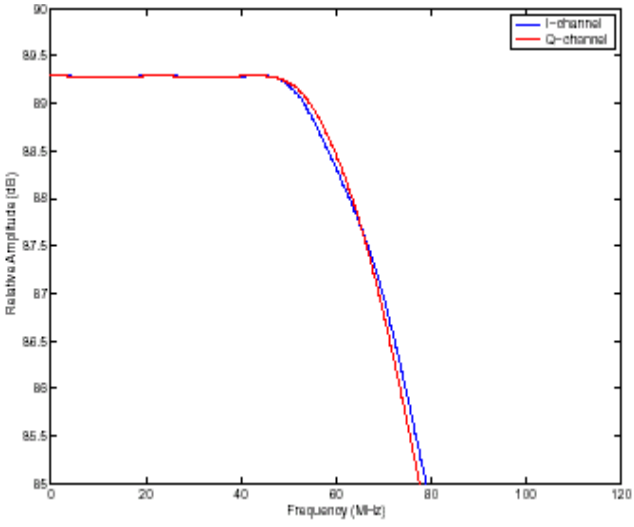

FIGURE 30A. TOTAL GAIN RESPONSE

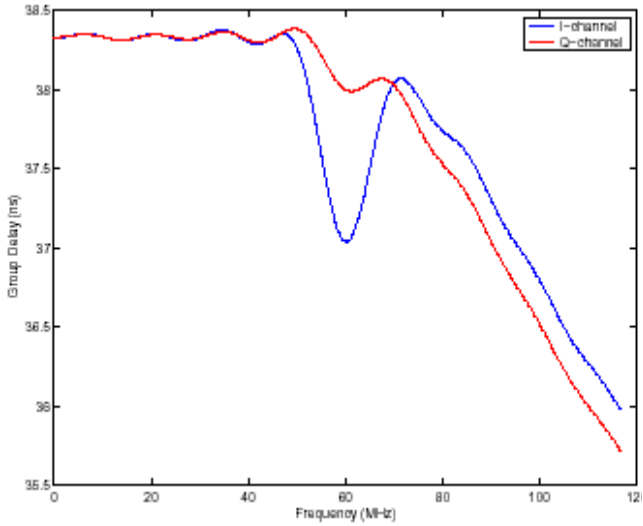

FIGURE 30B. TOTAL RESPONSE OF CASCADED FILTERS

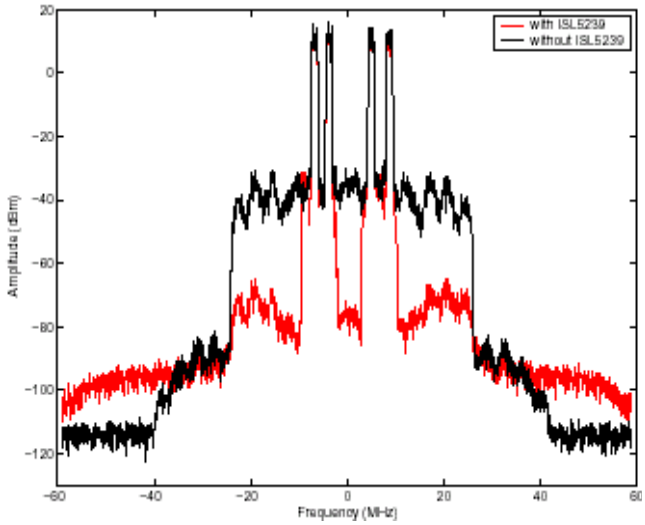

FIGURE 31A. FREQUENCY RESPONSE IMBALANCE WITHOUT CORRECTION

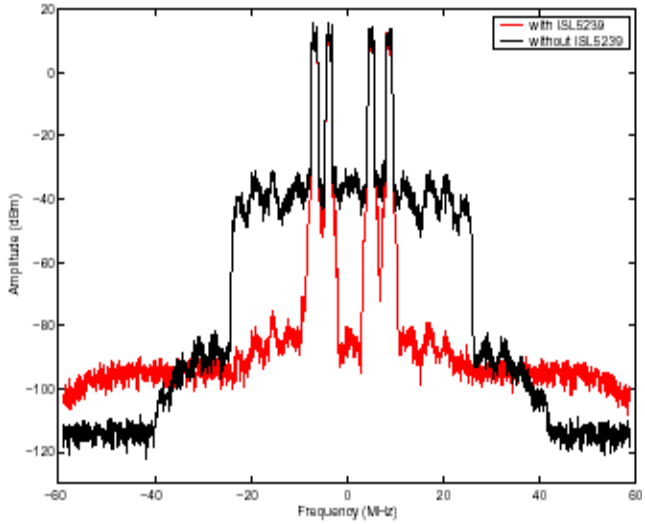

FIGURE 31B. FREQUENCY RESPONSE IMBALANCE WITH CORRECTION

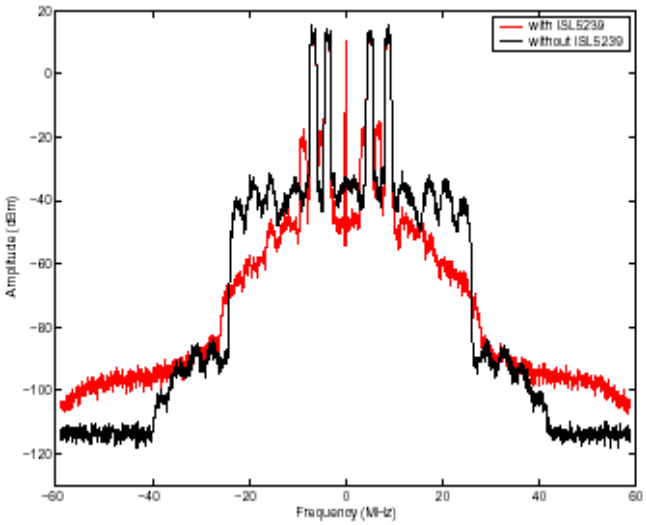

FIGURE 32A. GAIN, PHASE, AND FREQUENCY RESPONSE IMBALANCE WITHOUT CORRECTION

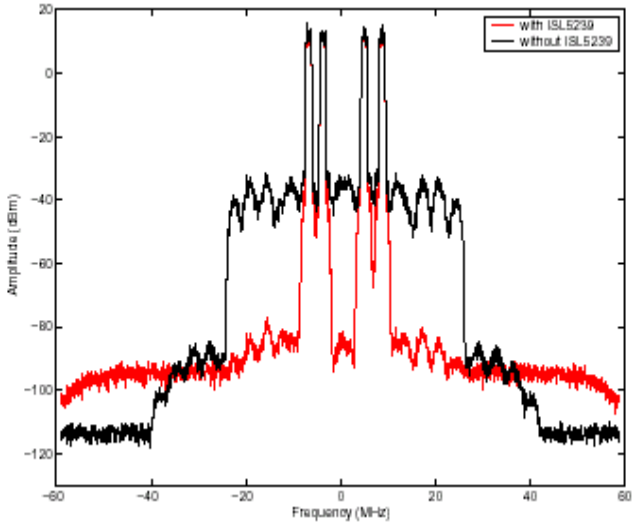

FIGURE 32B. GAIN, PHASE, OFFSET, AND FREQUENCY RESPONSE IMBALANCE WITH CORRECTION

IF Modes

The ISL5239 features three digital IF modes. These include complex, real 1x, and real 2x modes. In the complex and real 1x modes, signal bandwidth is half of that for the ZIF mode. Therefore, the examples that follow for complex IF and real 1x modes will only include carriers at 1.25 MHz and -3.75 MHz.

Figure 33A shows the performance in the complex IF mode with gain, phase, offset and frequency response imbalance. The spectrum is shown at baseband so the distortion due to DC offset appears at -30 MHz. Figure 33B shows the response when we correct for these imbalances. Evident are residual image components near ±60 MHz. These are larger than those encountered at ZIF because the correction filter performance degrades in the neighborhood of the transition bandwidth, which is where the IF signal resides. In particular, the signal in this case suffers from the mismatch shown in Figure 30 in the neighborhood of 30 MHz. The performance in removing IM distortion is limited for the same reason.

The real IF modes do not encounter imbalance problems since they are not used with direct upconversion. However, there are times when these modes require equalization to remove analog circuit effects -- for example sin(x)/x correction. The I-channel filter that was used to model frequency response imbalance above will serve as an example of a filter with non-flat frequency response. Figure 34A shows the performance in the real 1x IF mode with the I-channel filter distortion. Figure 34B shows the response with correction. Correction of IM components is limited due to the same reason discussed above -- the signal is in the neighborhood of the transition band where the correction filter performance is limited.

The signal bandwidth in the real 2x IF mode is the same as that for ZIF. Figure 35A shows the performance in the real 2x IF mode with frequency response distortion. Figure 35B shows the response with correction. The performance is comparable to that for ZIF shown in Figure 32B with small degradation due to limits on the correction filter performance in the neighborhood of the transition band.

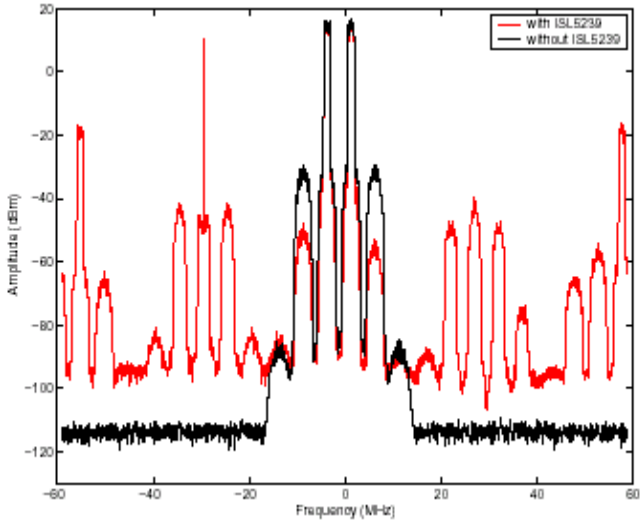

FIGURE 33A. GAIN, PHASE, OFFSET, AND FREQUENCY RESPONSE IMBALANCE WITHOUT CORRECTION

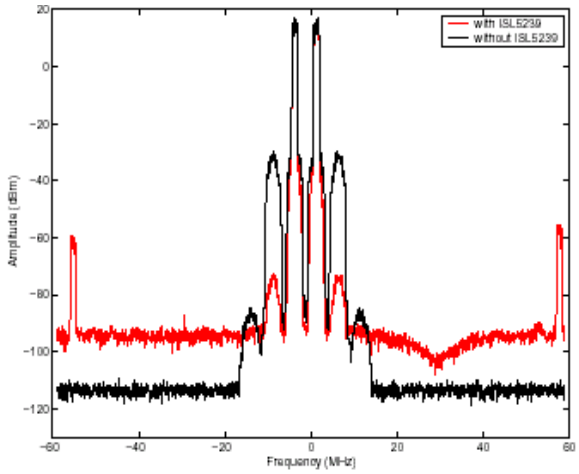

FIGURE 33B. GAIN, PHASE, OFFSET, AND FREQUENCY RESPONSE IMBALANCE WITH CORRECTION

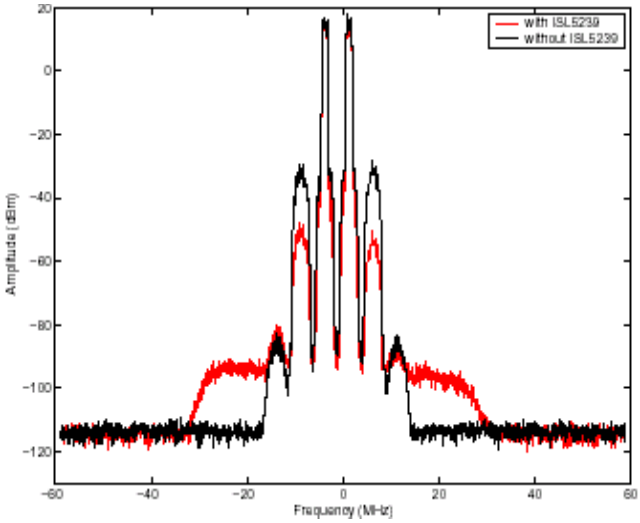

FIGURE 34A. FREQUENCY RESPONSE DISTORTION WITHOUT CORRECTION

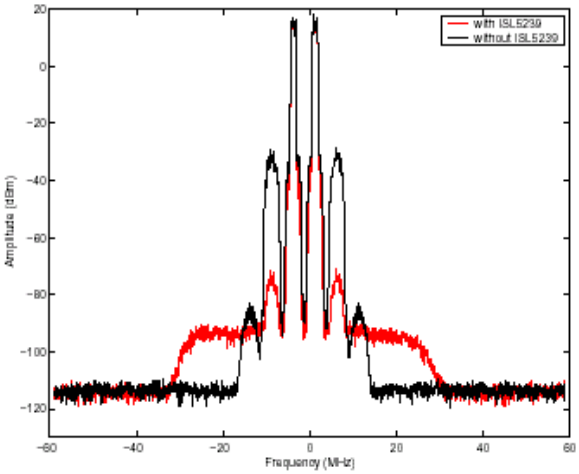

FIGURE 34B. FREQUENCY RESPONSE DISTORTION WITH CORRECTION

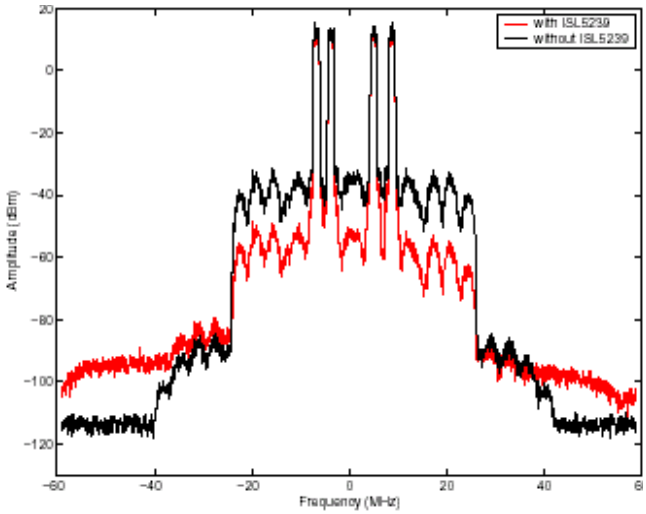

FIGURE 35A. FREQUENCY RESPONSE DISTORTION WITHOUT CORRECTION

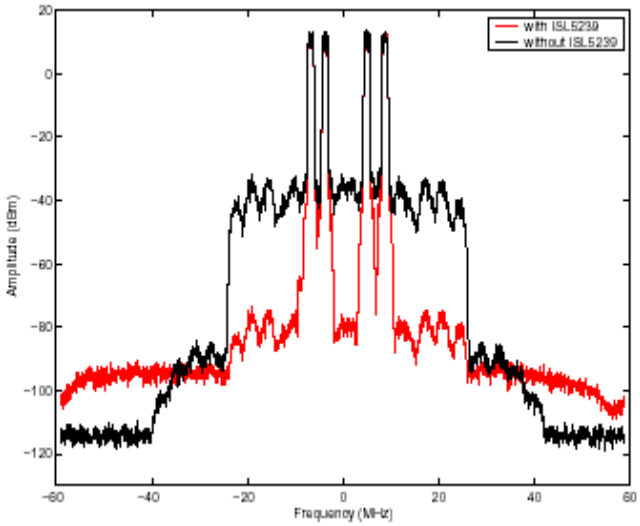

FIGURE 35B. FREQUENCY RESPONSE DISTORTION WITH CORRECTION

Memory Compensation

In this section we investigate the ISL5239's features for memory effect compensation. We first present the features in the predistortion linearizer for memory compensation. We describe how this architecture applies to the problem of self heating and then illustrate its use with an example.

ISL5239 Architecture

Figure 36 shows the PD function with the thermal compensation features. This figure shows a second LUT that adds a perturbation to the value from the first LUT. As a convention, we identify the two LUTs as nominal and delta. The perturbation from the delta LUT is scaled by a factor proportional to the magnitude of the memory effect. This technique can compensate for distortion caused by fast memory effects such as gain droop caused by thermal self heating described in [3]. The scale factors are shown in the A and B registers in the lower right portion of the figure. The

values in these registers are loaded through the serial port from an external device as shown. Another serial port is provided for exporting the calculated signal power to the external device. The external device uses the signal power along with any other measurements that are correlated with self heating (for example bias current or junction temperature) to predict the magnitude of the memory effect. The serial port provides updates to the A and B registers about once ever 8 μs, which is sufficient for correcting memory effects with 1 ms time constants or faster.

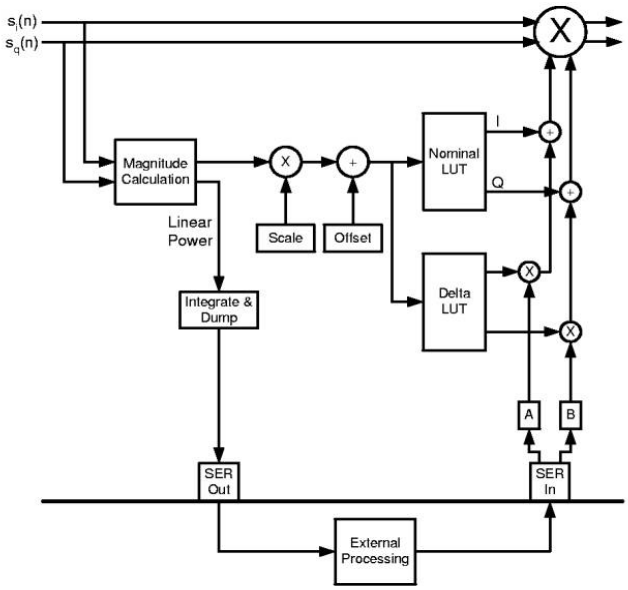

FIGURE 36. PREDISTORTION WITH THERMAL COMPENSATION

Operation and Performance

In Figure 3 we showed the AM-AM and AM-PM characteristics of an amplifier. We did not mention earlier that these characteristics will vary as a function of temperature. Figure 37 shows a family of AM-AM and AM-PM characteristics where each characteristic represents the amplifier's behavior at a given temperature. The upper-most characteristic governs the amplifier behavior at a low temperature and the lower-most characteristic governs it at a high temperature. Then N = 20 characteristic curves shown in Figure 37 are defined by:

$$g_a(|Vi(t)|^2, n) = a_1(n) + a_2(n)|Vi(t)|^2 + a_3(n)|Vi(t)^4|,$$

$$n = 1, 2, 3,., N \quad \text{(EQ.6)}$$

$$g_\Phi(|Vi(t)|^2, n) = b_1(n) + b_2(n)|Vi(t)|^2 + b_3(n)|Vi(t)^4|,$$

$$n = 1, 2, 3,..., N \quad \text{(EQ.7)}$$

where:

$a_1(n) = 10 - [2(n-1) / N]$

$a_2(n) = -10 - [2(n-1) / N]$

$a_3(n) = 7(n-1) / N$

and

$b_1(n) = 0$

$b_2(n) = -0.3 - [0.2(n-1) / N]$

$b_3(n) = 0$

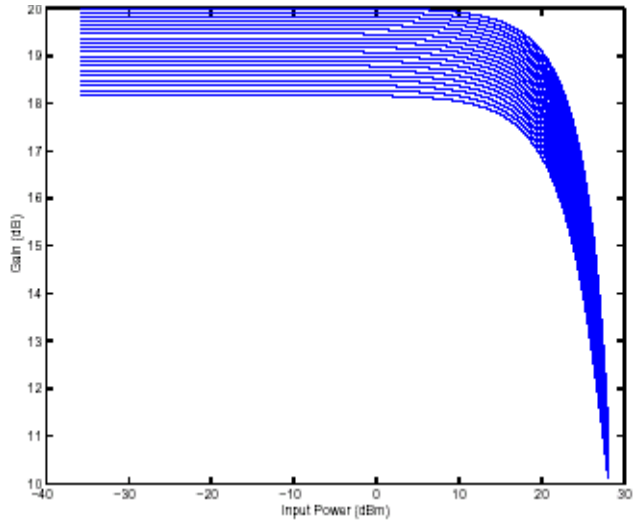

FIGURE 37A. CHARACTERIZATION OF A NONLINEARITY WITH MEMORY (AM-AM CHARACTERISTICS)

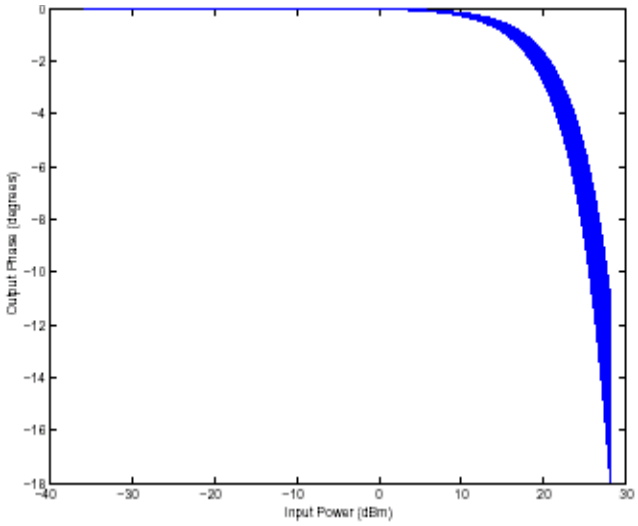

FIGURE 37B. CHARACTERIZATION OF A NONLINEARITY WITH MEMORY (AM-PM CHARACTERISTICS)

There are a number of issues to consider when linearizing an amplifier that is governed by a family of curves. For one, where should one define the linear response? Figure 38 shows a linear response that coincides with the upper-most characteristic. This response results in a PA with maximal gain and therefore maximum power added efficiency (PAE). The operating region is determined by the curve with the minimum saturation level, as shown in the figure. The upper-most characteristic will serve as our nominal curve, so the nominal LUT values are the same as before for memoryless linearization. Our focus turns now to the delta LUT.

The ISL5239 delta LUT is comprised of 1024 entries of I and Q values each quantized to 14 bits signed, which provides a perturbation region of -2^{13} to $+2^{13}$ - 1 centered on the nominal vector as shown in Figure 39. The delta pertebation can be used to move the nominal correction vector anywhere within the shaded region of the figure.

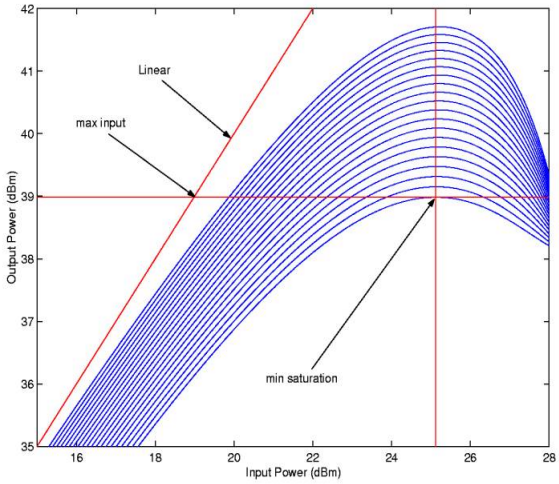

FIGURE 38. AM-AM CHARACTERISTICS

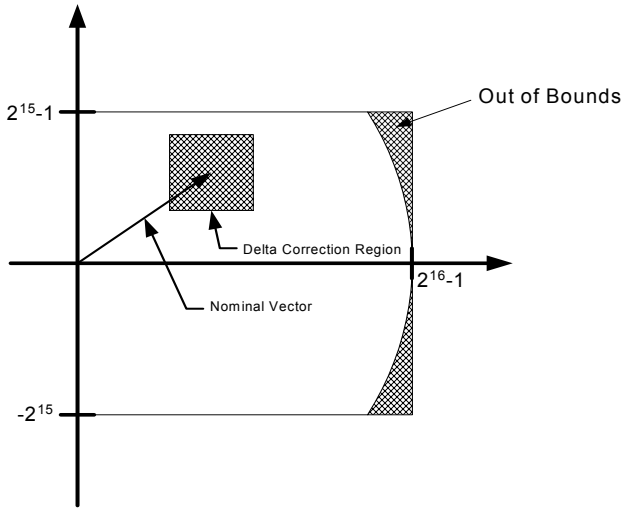

FIGURE 39. LUT VECTOR SUBSPACE WITH DELTA CORRECTION

The thermal variation shown in Figure 37 is too large to accommodate with the delta LUT directly. The quantization within the delta LUT is only sufficient to accommodate a subset of the family of characteristics. Figure 40 shows a subset of the AM-AM and AM-PM characteristics. In particular, this subset includes the first four curves (n = 1,..., 4). The nominal curve is defined by n = 1and the delta curve by n = 4 as indicated in the figure.

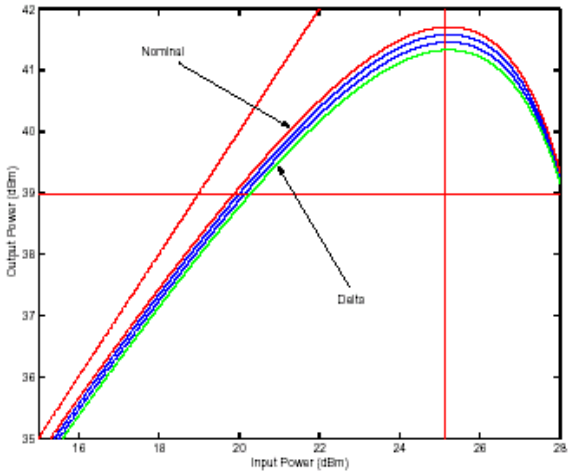

FIGURE 40A. NOMINAL AND DELTA CURVES (AM-AM CHARACTERISTICS)

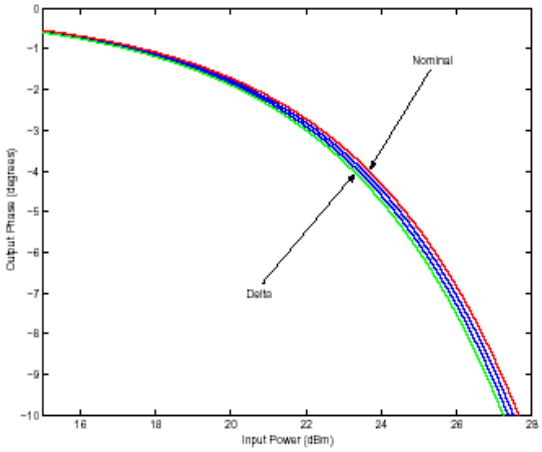

FIGURE 40B. NOMINAL AND DELTA CURVES (AM-PM CHARACTERISTICS)

With the nominal and delta curves defined, we turn our attention to the generation of the table for the delta LUT. The nominal LUT was discussed in “Linearization Fundamentals” on page 1, and is shown in Figure 15. Suppose that the PA temperature is such that the delta characteristic governs the amplifier behavior. As such, the interpolation scale factors are a = 1 and b = 1. Let Vi denote the PD input and let $ViG_Re^{j\Phi_R}$ denote the required PA input. Let $G_Ne^{j\Phi_N}$ and $G_\Delta e^{j\Phi_\Delta}$ denote the nominal and delta LUT values. It can be easily shown that the delta LUT values are given by:

$$G_\Delta = \sqrt{x^2 + y^2}$$

$$\phi_\Delta = \text{atan}\frac{y}{x}$$

where:

$$x = G_R\cos(\Phi_R) - G_N\cos(\Phi_N) \quad \text{(EQ.8)}$$

$$y = G_R\sin(\Phi_R) - G_N\sin(\Phi_N) \quad \text{(EQ.9)}$$

Figure 41 shows the gain and phase of the delta LUT calculated from (9). The delta LUT gain is small over the linear range and increases in the compression region. The phase behaves in a similar fashion.

Figure 42 shows the performance improvement that is gained by incorporating the delta LUT. In this case the amplifier is governed by the 4th characteristic curve and the delta LUT is that given in Figure 41.

When the amplifier is governed by a characteristic curve that fall between the nominal and the delta curve, then the a and b parameters shown in Figure 36 are used to interpolate between the characteristic curves. Figure 43 shows the interpolated curve along with the actual model values for the example given. In this case simple linear interpolation was used where a = b and the estimate is very good. Other interpolation techniques are possible and may be appropriate depending on the PA model.

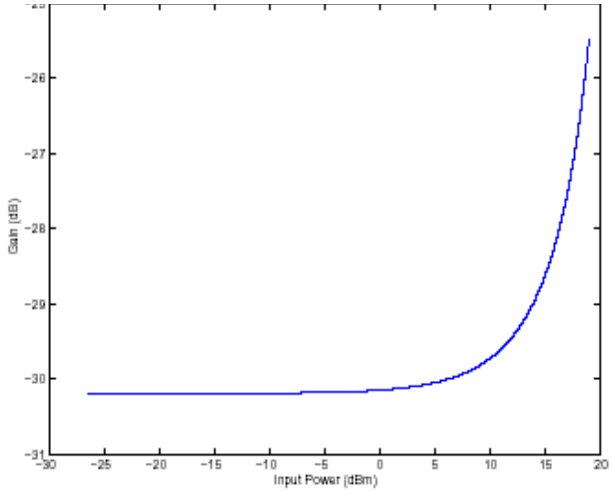

FIGURE 41A. DELTA LUT GAIN CHARACTERISTICS

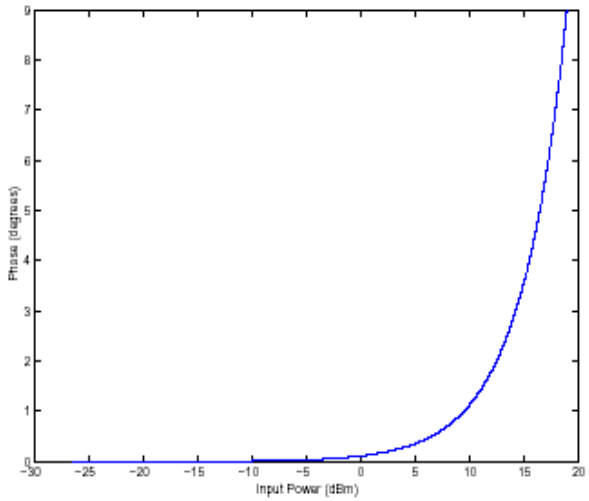

FIGURE 41B. DELTA LUT PHASE CHARACTERISTICS

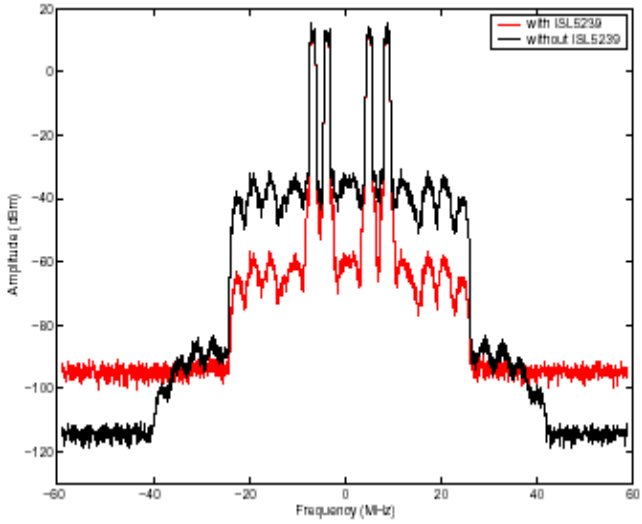

FIGURE 42A. PERFORMANCE WITHOUT DELTA LUT

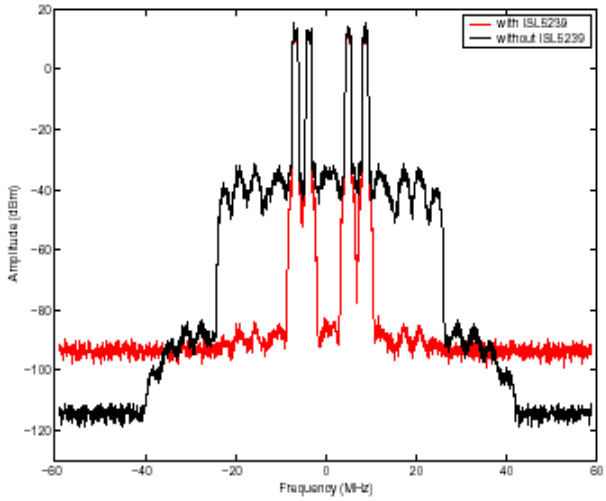

FIGURE 42B. PERFORMANCE WITH DELTA LUT

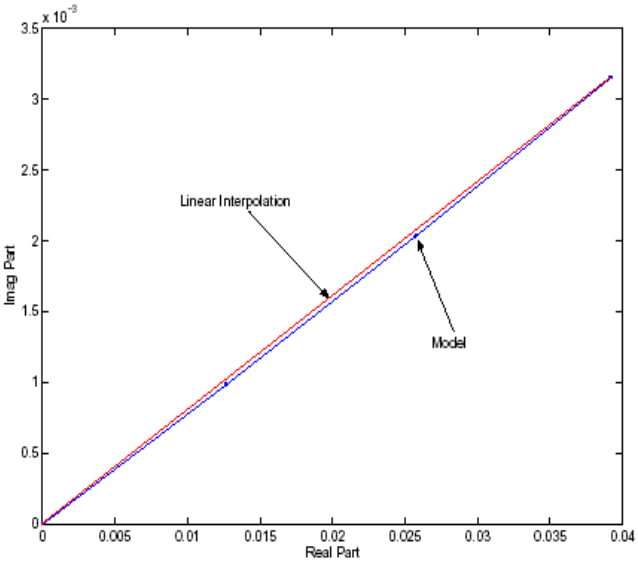

FIGURE 43. DELTA TABLE INTERPOLATION

As a final example, we consider thermal compensation due to self heating. In this case the input power level is switched between high and low levels. The input power level is shown in Figure 44A. This figure shows that the signal power level is switched between a high and low level every 2 ms. There is a 13 dB difference between the high and low power levels. Figure 44B shows the amplifier's temperature variation in response to the input power fluctuations. The PA thermal time constant is around 2 ms and is governed by a 8th order Butterworth LPF. Figure 44C through 44K show the PD performance with and without thermal compensation at each 1 ms increment in time. These figures show that the performance without thermal compensation is severely degraded when the amplifier is operated at high temperature and high power, while the performance with thermal compensation is unaffected by temperature variation.

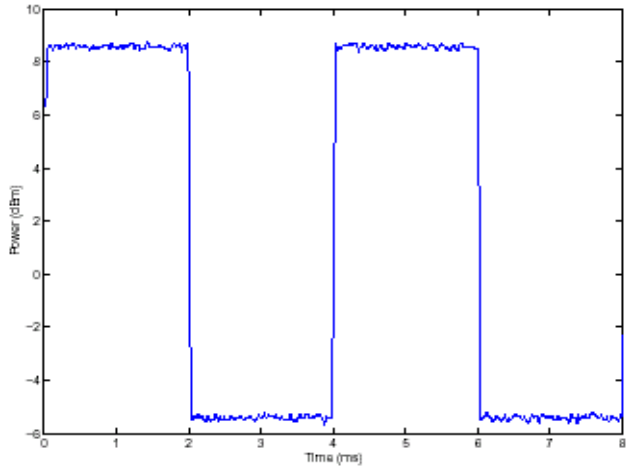

FIGURE 44A. INPUT SIGNAL POWER (THERMAL COMPENSATION FOR SELF HEATING)

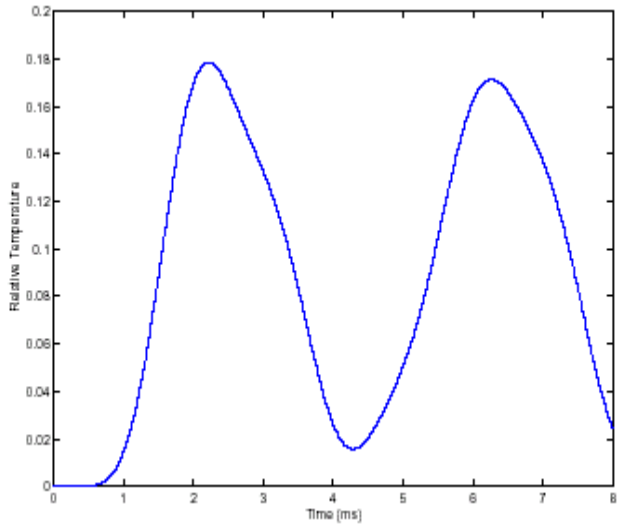

FIGURE 44B. AMPLIFIER TEMPERATURE (THERMAL COMPENSATION FOR SELF HEATING)

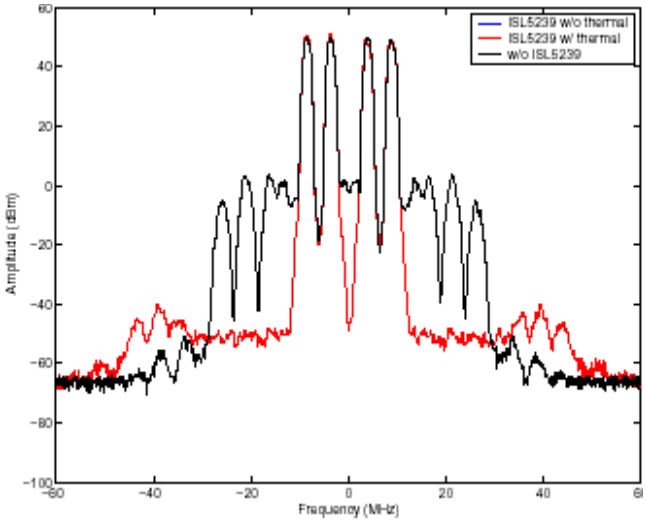

FIGURE 44C. SPECTRUM AT t = 0 ms (THERMAL COMPENSATION FOR SELF HEATING)

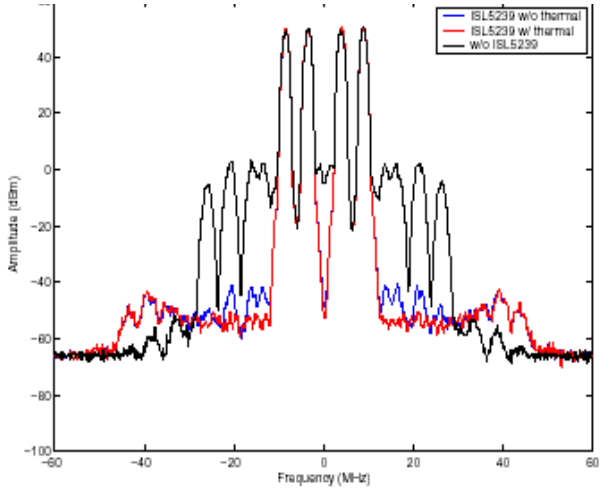

FIGURE 44D. SPECTRUM AT t = 1 ms (THERMAL COMPENSATION FOR SELF HEATING)

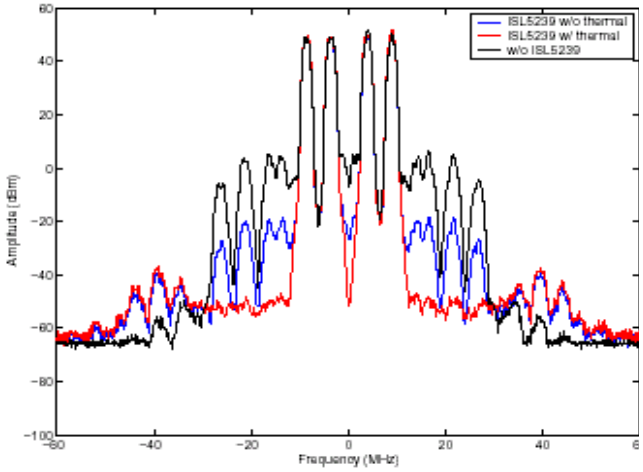

FIGURE 44E. SPECTRUM AT t = 2 ms (THERMAL COMPENSATION FOR SELF HEATING)

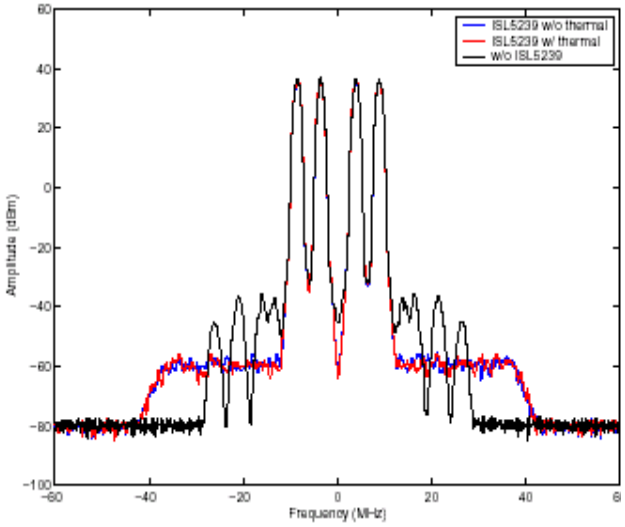

FIGURE 44F. SPECTRUM AT t = 3 ms (THERMAL COMPENSATION FOR SELF HEATING)

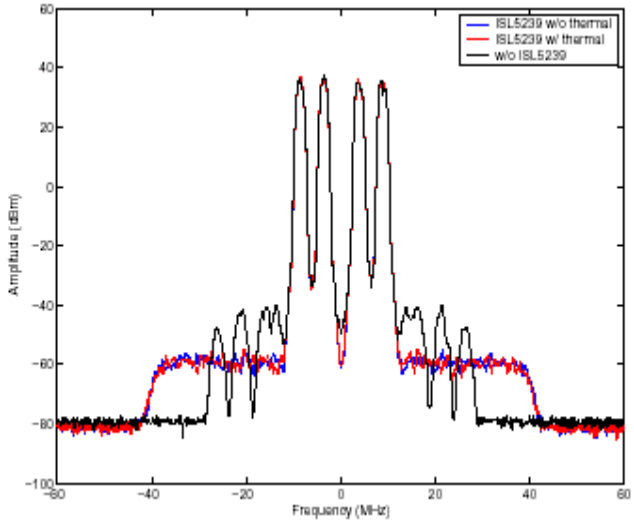

FIGURE 44G. SPECTRUM AT t = 4 ms (THERMAL COMPENSATION FOR SELF HEATING)

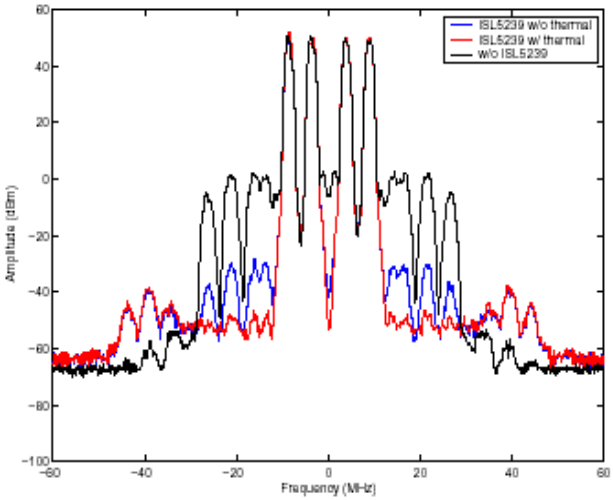

FIGURE 44H. SPECTRUM AT t = 5 ms (THERMAL COMPENSATION FOR SELF HEATING)

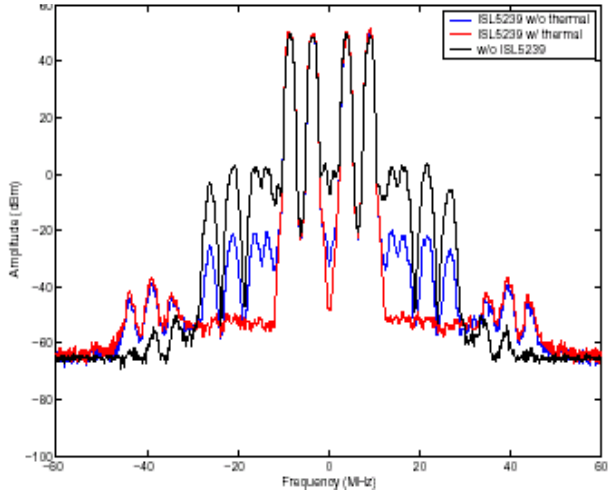

FIGURE 44I. SPECTRUM AT t = 6 ms (THERMAL COMPENSATION FOR SELF HEATING)

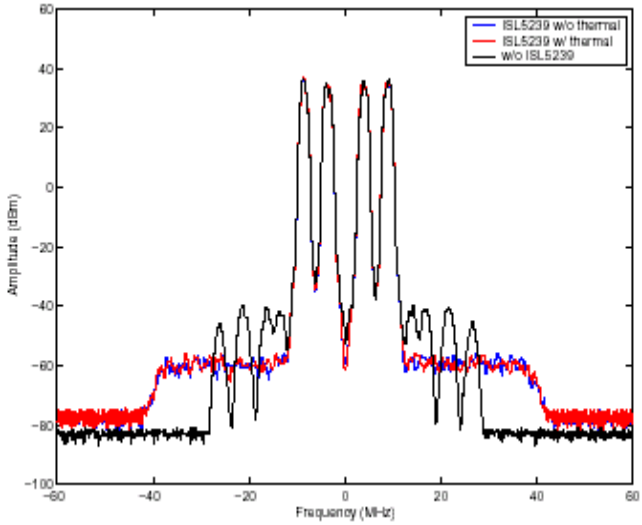

FIGURE 44J. SPECTRUM AT t = 7 ms (THERMAL COMPENSATION FOR SELF HEATING)

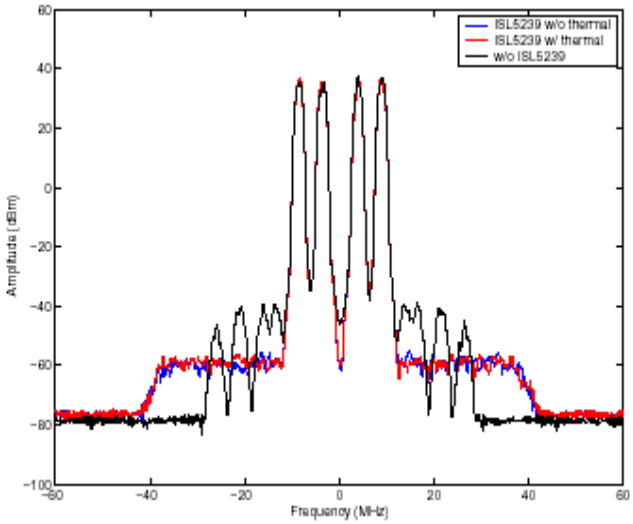

FIGURE 44K. SPECTRUM AT t = 8 ms (THERMAL COMPENSATION FOR SELF HEATING)

Summary

The purpose of this application note was to present the features and describe the operation and performance of the ISL5239 PDL. We began with a tutorial on linearization fundamentals in “Linearization Fundamentals” on page 1. In “Memoryless Nonlinearity” on page 2, we described the ISL5239 architecture covering the many features of the part including: (1) interpolation; (2) addressing modes; (3) PD LUT; (4) IF modes; (5) correction filter; (6) and imbalance and offset correction. The performance of each of these features was investigated in “Memoryless Nonlinearity” on page 2. The features for correcting thermal memory effects were described in “Memory Compensation” on page 18. The procedure for generating the delta LUT from the amplifier’s characteristic curves was given. This section included an example showing the correction of gain droop on pulsed waveforms due to self heating.

In summary, the advanced features included in the ISL5239 constitute an enabling break-through for digital predistortion. At present, it is the lowest-cost full-featured part available for adaptive digital linearization, for either quadrature or digital IF upconversion architectures. It addresses common shortcomings of other digital linearizers in the correction of frequency response and memory effect errors. More efficient and reliable multi-carrier transmitters are enabled by eliminating the need for complex analog upconversion and feedforward PA linearization circuits. Although we didn’t address it here, manufacturability is facilitated by digital self-calibration methods. Finally, the part enables simpler, and more cost effective overall transmitter designs for UMTS, CDMA2000, and other 3G applications.

References

[1] S. C. Cripps, RF Power Amplifiers for Wireless Communication, Artech House, 1999.

[2] J.K. Cavers and M.W. Liao, Adaptive Compensation for Imbalance and Offset Losses in Direct Conversion Transceivers, IEEE Trans. Veh. Tech., vol. 42, no. 4, pp. 581-588, 1993.

[3] W. Bosch and G. Gatti, Measurement and Simulation of Memory Effects in Predistortion Linearizers, IEEE Trans. Microwave Theory and Techniques, vol. 37, no. 12, pp. 1885- 1890, 1989.